FLOW RATE CONTROL SYSTEM UTILIZING RHEOLOGICAL PARAMETERS FOR PRECISE AND CONSISTENT EXTRUSION IN 3D CONCRETE PRINTING

A Thesis

by

Oğulcan Ahi

Submitted to the
Graduate School of Sciences and Engineering
In Partial Fulfillment of the Requirements for
the Degree of

Master's Degree

in the
Department of Mechanical Engineering

Özyeğin University
July 2023

FLOW RATE CONTROL SYSTEM UTILIZING RHEOLOGICAL PARAMETERS FOR PRECISE AND CONSISTENT EXTRUSION IN 3D CONCRETE PRINTING

Approved by:

Assist. Prof. Özkan Bebek, Advisor
Dept. of Mechanical Eng.
Özyeğin University

Assoc. Prof. Özgür Ertunç
Dept. of Mechanical Eng.
Özyeğin University

Assoc. Prof. Çağla Meral Akgül
Dept. of Civil Eng.
Middle East Technical University

Date Approved: 27 July 2023

To my family

ABSTRACT

The use of inline quality assessment technologies is of great importance in meeting the consistent extrusion requirements of 3D concrete printing (3DCP) applications. The proposed study suggests a system for regulating the extrusion speed during 3DCP processes in order to maintain the extrusion flow rate at a targeted value. This system is based on a newly proposed equation that combines both printing parameters and the rheological properties of the material used in the printing process. The study presents a novel flow rate control method for 3DCP, leveraging a unique correlation between printing and rheological parameters, to address quality assessment strategies in the process. The control strategy that has been proposed is established to function effectively with different types of cement-based mixtures and has the capability to regulate the extrusion process, thereby ensuring the attainment of a targeted flow rate from the system. Validation tests demonstrate that the proposed flow rate control can maintain an instantaneous flow rate within a certain range and eventually achieve a constant flow rate. During operation, the flow rate is consistently maintained around the targeted value with an average error rate of 6.7 percent. The presented flow rate control mechanism exhibits promising potential as a reliable and efficient solution for achieving precise and constant flow rate values, regardless of the cement mix design employed.

ÖZETÇE

3D beton baskı (3DCP) uygulamalarında ekstrüzyon kalitesinin devamlılığını sağlamak için hat içi kalite değerlendirme teknolojilerinin kullanımı büyük öneme sahiptir. Bu çalışma, 3DCP süreçlerinde ekstrüzyon hızını düzenlemek için bir sistem önermektedir, böylece ekstrüzyon akış hızını hedeflenen bir değerde tutmayı sağlar. Bu sistem, baskı parametrelerini ve baskı sürecinde kullanılan malzemenin reolojik özelliklerini birleştiren yeni bir denklem temelinde oluşturulmuştur. Çalışma, baskı ve reolojik parametreler arasındaki benzersiz ilişkiyi kullanarak 3DCP için yeni bir akış hızı kontrol yöntemi sunmakta ve süreçte kalite değerlendirme stratejileri ele alınmaktadır. Önerilen kontrol stratejisi, farklı tipte çimento bazlı karışımlarla etkin bir şekilde çalışacak şekilde geliştirilmiş olup, sistemden hedeflenen akış hızının elde edilmesini sağlayarak ekstrüzyon sürecini düzenleme kapasitesine sahiptir. Yapılan testlere göre geliştirilen sistemin, çimento ekstrüzyon hızını belirli bir aralıkta tutabildiği ve sonunda sabit bir akış hızı elde edilebildiği görülmüştür. Ekstrüzyon işlemi sırasında, akış hızı hedeflenen değerin etrafında sürekli olarak korunmakta olup, ortalama hata oranı %6,7'dir. Sunulan akış hızı kontrol mekanizması, kullanılan çimento karışımı tasarımından bağımsız olarak hassas ve sabit akış hızı değerleri elde etmek için güvenilir ve verimli bir çözüm olarak umut vadetmektedir.

ACKNOWLEDGEMENTS

I would like to begin by expressing my gratitude to my advisor, Özkan Bebek, who not only provided me with the initial opportunity to embark on this research but also extended unwavering support throughout these years. His encouragement and understanding nature as a mentor have been invaluable to me, and I am confident that anyone fortunate enough to know him would share the same sentiment. I am truly grateful for his continuous motivation, which played a pivotal role in enabling me to successfully complete this work.

Additionally, I want to express my sincere gratitude to my other mentors, Özgür Ertunç and Zeynep Başaran Bundur, who played a crucial role, almost like co-advisors, in the success of this study. Their guidance and unwavering support were instrumental in overcoming challenges along the way. Whenever a problem arose, they were readily available to assist me in finding solutions. I am deeply grateful for their contributions, and I know that their impact will stay with me throughout my life. I wish them all the best in their future endeavors.

I would like to express my gratitude to my labmates Ahmet Burhan Kara, Ilgın Sandalcı, Shaghayegh Benam, and Tolga Aydın for their friendship and help throughout the test sessions of this study. Also, I am thankful to all those who supported me during this research. Your encouragement and belief in my work have been truly uplifting. Thank you all for being a part of this journey with me.

Furthermore, I extend my thanks to Çağla Meral Akgül for being a valuable part of my jury.

Above all, I would like to express my biggest thanks to my family for their unwavering love, guidance, and motivation, which have played a pivotal role in shaping

me into the person I am today.

This work was supported by the Scientific and Technological Research Council of Turkey (TUBITAK) under Grant No. 119M520.

Nomenclature

Greek Letters

μ	Dynamic viscosity
ν	Kinematic viscosity
ω	Angular velocity
ω_0	Initialized angular velocity
Π	Non-dimensional numbers
ρ	Density
τ	Shear stress
τ_0	Yield stress

Acronyms and abbreviations

CAD	Computer Aided Design
CSR	Controlled Shear Rate
DC	Direct Current
FA	Fly Ash
GNF	Generalized Newtonian Fluid
HB	Herschel Bulkley
LHS	Left Hand Side
OPC	Ordinary Portland Cement

RHS Right Hand Side

rpm Rotation Per Minute

VMA Viscosity Modifying Agent

ZOH Zero Order Hold

Physics constants

ΔP Pressure drop

$\dot{m}_{ref}$ Reference mass flow rate

$Q_{derived}$ Flow rate calculated using established equation

Q_{meas} Flow rate measured with gravimetric measurement technique

Q_{ref} Reference flow rate

p Proportional gain

T Temperature

a,b,c Constants

D Nozzle Edge Length

k Viscosity index

L Distance between pressure sensors

l Length

M Primary dimension of mass

n Flow index

P Pressure

Q	Flow rate
R	Cylindirical tube radius
T	Torque
t	Time
V	Flow velocity

TABLE OF CONTENTS

DEDICATION . . . . **iii**

ABSTRACT . . . . **iv**

ÖZETÇE . . . . **v**

ACKNOWLEDGEMENTS . . . . **vi**

LIST OF TABLES . . . . **xiii**

LIST OF FIGURES . . . . **xiv**

I INTRODUCTION **1**

1.1 Previous Studies related to extrusion quality control 6

1.2 Scope, goals and significance of the thesis 14

1.3 Thesis Structure 16

II METHODOLOGY **19**

2.1 Dimensionless group selection 19

2.2 Simulation of the 3DCP process 24

2.2.1 Model simulation 24

2.2.2 Physical model selection and mesh operation 26

2.2.3 Data collection process and convergence criterion 28

2.2.4 Simulation Analysis 30

2.3 Experimental setup 35

2.4 Material selection and analysis 39

2.5 The test procedure and data collection 41

2.5.1 Preparation and Calibration 41

2.5.2 Experiment 42

2.5.3 Post-process 42

2.6 Correlation investigation of non-dimensional pair 43

2.7 Numeric solution of Q for quality control 49

2.8 Controller Implementation 50

III EXPERIMENTAL VERIFICATION AND DISCUSSION 53

3.1 Performance Evaluation of Derived Flow Rate 53

3.2 Comparison of Measured and Derived Flow Rates 60

IV CONCLUSIONS 63

REFERENCES 69

VITA 76

LIST OF TABLES

1 Selected physical parameters of an extrusion system 23

2 Properties and specifications of the experimental setup 38

3 The goodness of fit scores (R^2) of selected non-dimensional pairs . . . 46

4 Flow rate control model test results under different test conditions . . 61

LIST OF FIGURES

1 StarCCM+ screen displaying the meshed part of the extrusion system 24

2 Dynamic viscosity vs shear rate analysis 27

3 Geometric scene of the simulation 29

4 Residual error plot 30

5 The pressure drop across the tube during cement extrusion for different cement types and rotation rates. 32

6 The variation in dynamic viscosity during cement extrusion for different cement types and rotation rates. 34

7 The overview of the cement extrusion setup 36

8 Technical representation of the test setup 37

9 Shear stress vs shear rate plot of cement sample from 0 to 60 minutes 40

10 The flow diagram of the experimental procedure 42

11 The plots of all 4 regression techniques applied on Π_1 and Π_2. 45

12 The relationship between non-dimensional groups Π_1^2 and Π_2. 48

13 The controller block diagram to regulate the angular velocity. 50

14 Recorded data of a flow rate control system test trial. 55

15 The histogram plots of collected signal data 56

16 The box plot of derived flow rate values using the control system . . . 57

17 Collected mass flow rate values during experiments. 59

18 The error bar plot according to T-distribution. 62

CHAPTER I

INTRODUCTION

Autonomously controlled intelligent systems are increasingly being utilized in the construction industry to improve the efficiency of construction operations in terms of time, cost, and safety [1, 2, 3, 4]. One of the key advantages of these systems is their ability to eliminate the human factor, which can lead to errors, accidents, and delays in construction projects.

Such intelligent systems can perform basic tasks including material handling and demolition [5, 6, 7, 8] as well as more complex tasks including inline and outline quality assessment via utilizing sensors, cameras, and machine learning algorithms to analyze data from construction sites, identifying patterns and trends that can help improve construction processes over time [9, 10, 11, 12].

One of the most commercially observed digital technologies in construction is 3D concrete printing (3DCP) [13, 14, 15]. The main application of 3DCP processes is to use layer-by-layer concrete extrusion for creating buildings and complex-shaped structures [16]. Whilst the implementation of 3DCP in field applications reduces the total cost of construction [17]; it also improves the safety and rate of construction compared to the conventional casting techniques [2].

The initial implementation of automated construction was introduced in 1997 [18], when Joseph Pegna introduced the concept of AM (Additive Manufacturing) for automated layer-by-layer construction of structures. Following this breakthrough, numerous researchers have dedicated their efforts to the study of digital construction. Various construction techniques, including Contour Crafting, D-Shape, and concrete printing, have been employed in the exploration of this field since 1997.

The Contour Crafting technique was developed and commercialized by researchers at the University of Southern California, and it has been utilized for the construction of 3D printed housing structures [19]. This technique represents a departure from the earlier research conducted by Pegna, as it involves the use of a pre-mixed material that can harden once it is extruded onto the surface. This innovation simplifies the construction process and enables the integration of essential electrical and drainage channels within the structure. Subsequent research conducted on the Contour Crafting technique has revealed its capability to produce structures with more intricate geometries. This advancement has been a significant finding in the field. By leveraging the Contour Crafting method, researchers have demonstrated the ability to construct buildings and structures with complex shapes and designs that were previously challenging to achieve using traditional construction methods. The flexibility and precision offered by the Contour Crafting technique have opened up new possibilities for architectural innovation and design. Extensive research has been conducted to investigate the environmental impacts of the Contour Crafting technology. These studies have highlighted several potential advantages associated with this automated construction technique. Some research studies [20] claim that utilizing this technology can lead to a remarkable reduction in construction waste, with potential waste reduction rates of up to 100%. This reduction in waste can contribute significantly to mitigating environmental pollution caused by traditional construction methods. Furthermore, the economical advantages of Contour Crafting have also been explored. Research findings indicate that this technology has the potential to benefit low-income countries by lowering construction costs. By streamlining the construction process and reducing labor requirements, Contour Crafting enables more cost-effective building construction. This affordability factor can greatly assist low-income countries in facilitating easier access to quality housing and infrastructure. Overall, the investigation of environmental and economic impacts has highlighted the potential of Contour

Crafting as a sustainable and economically viable construction method.

Concrete printing can be considered as a simplified version of Contour Crafting, with minor differences observed in the surface finish of the printed product [21]. One key distinction is that Contour Crafting typically produces a smoother surface finish compared to concrete printing. While both methods involve the layer-by-layer extrusion of concrete materials, Contour Crafting offers more precise control and finer details in the construction process. This enhanced precision allows for the creation of smoother surfaces with a higher level of accuracy. In contrast, concrete printing techniques may have some limitations in achieving the same level of surface smoothness. However, concrete printing still offers significant advantages in terms of construction speed, cost-efficiency, and the ability to create basic structural elements.

The D-Shape method is an alternative automated construction technique developed by Enrico Dini in 2008 [22]. In contrast to Contour Crafting, this method allows for the construction of complex shapes with irregular cross sections. While Contour Crafting requires constant cross-sectioned layers, the D-Shape method utilizes the outer frame of the structure as a reference and prints the components accordingly. The process involves detecting the contour of the object for each layer and creating a tool path accordingly. Cement extrusion takes place along this path, and the procedure is repeated layer by layer until the desired part or structure is completed. This approach enables the construction of more intricate geometries and non-uniform shapes, expanding the possibilities for architectural design and customization. The D-Shape method represents a unique advancement in automated construction, providing increased flexibility in shaping the printed structures while maintaining the benefits of additive manufacturing.

The studies on automated construction techniques, such as 3D concrete printing, demonstrate that these technologies offer both economic and various other advantages. The economic advantages of 3D concrete printing arise from its potential to reduce construction costs through optimized material usage, decreased labor requirements, and streamlined construction processes. By automating certain aspects of construction, this technology can enhance efficiency and productivity while minimizing waste and expenses.

However, it is crucial to note that implementing 3D concrete printing requires specialized knowledge in materials science to develop suitable concrete mixes that can be extruded and maintain structural integrity. Additionally, expertise in the manufacturing process is necessary to ensure proper calibration and operation of the printing equipment. Also, continuous monitoring of the process is essential to ensure the quality of the printed structure [23].

The concrete printing process can be a revolutionary method for the architecture area but building such a system is rather complex and several points should be investigated with deep insight in order to get good, reliable results. Different types of errors may occur during this type of layered manufacturing process. The cold joint formation, layer collapsing failures, and under-filling are some common issues faced in the literature [13]. These issues should be addressed in advance in order to build stable structures. Layer collapsing failures happen due to the change in extrusion height which is the distance between the nozzle outlet and the working surface. While the building height advances, the hydro-static pressure increases, and the upper layers start to compress the lower ones. Consequently, both the extrusion height and the filament shape alter during the extrusion process, potentially leading to the structure's total failure. Layer collapsing failures is grown from the variations in the yield stress of the mixture while it is extruded [13]. Under-filling is another common problem where the extruded material becomes volumetric-wise insufficient for a duration of time. This situation can create voids in the building and thereupon it can decrease the overall strength of the structure. The main reason for this case is the lack of continuous feed rate control of the system. Another failure cause is cold joint formation which is due to layer adhesion issues and can create weak plane sections. The phenomenon of cold joint formation occurs when the layer cycle time is too long. Note that cycle time is highly dependent on printed filament geometry and process parameters [13]. However, this can be solved by continuous measurement and control of process parameters such as feed rate, viscosity, etc. In order to gain a more comprehensive understanding of the intricacies of this innovative method, it is essential to examine the topic through multiple categories or subtopics.

A notable challenge encountered in the system pertains to issues associated with materials [13], [24]. The effectiveness of extrusion-based construction highly depends on the rheology of the extruded material. In order to have a stable structure, these materials should have some specific rheological features (i.e. sufficient yielding stress, viscosity, etc.) [25]. The material characteristics of 3D concrete printing are currently being extensively researched. This includes investigations into the optimal cement composition for 3D printing processes, as well as the study of material effects on the build-ability and durability of layer-by-layer extrusion [26, 27, 28].

Another reason for having difficulties in 3DCP applications is the lack of a quality control system. Even with newly developed material compositions, operational problems such as over-filling, under-filling, and cold joint formation still do exist. Cement-based materials are highly complex and versatile. By nature, cementitious systems exhibit shear-thinning behavior such that these materials have a tendency to have lower viscosity values under the applied shear [29]. Since extrusion is a highly dynamic process, there is a continuous shear effect on the cement-based mixture which directly yields viscosity variations. Due to this variation of viscosity, the flow rate, extrusion pressure, and outlet viscosity of any extrusion process can vary by a significant amount. These variations create obscurities and inevitably affect the overall extrusion efficiency. Conventional quality assessment methods such as flow tables are insufficient for 3D concrete printing, as they are not applicable without disrupting the process.

1.1 Previous Studies related to extrusion quality control

The literature has frequently reported a lack of quality control in 3D concrete printing (3DCP), as evidenced by studies such as [23], [30], and [31]. To address this gap, a system for real-time measurement and control of extrusion height was proposed [32].The primary objective of this research was to develop a control method to mitigate a prevalent problem known as self-weight deformation, commonly encountered in 3D concrete printing (3DCP) applications. During the layer-by-layer extrusion of cement, the previously printed layers are subjected to significant deformation due to the weight exerted by the upper layers.

The deformation takes place due to the compression caused by the weight of the additional layers. As a result, the thickness of the initial layers tends to reduce under this compressive force. Consequently, with each deformation, the gap between the nozzle and the printed layers gradually widens, causing the cement to be extruded from a higher position. This results in instability in the layers extruded at greater heights, thereby compromising the overall structural integrity.

This phenomenon, known as deformation due to self-weight, has a detrimental effect on the stability of the printed structure as a whole. The study emphasizes the importance of monitoring various aspects of the printing process and utilizing acquired data to provide real-time feedback for achieving optimal print results. In order to facilitate future extensions of the idea, the nozzle height is selected as the target parameter. The nozzle height, denoted as h_{nozzle}, is defined as the vertical distance between the last printed cement layer and the tip of the extrusion nozzle. To measure the nozzle height, a 1D Time of Flight (ToF) Distance sensor is employed. This sensor, located at the print head, enables real-time measurements with an accuracy of approximately 1 mm and a range of up to 200 mm. The data collected by the sensor is collected and transmitted to a control unit via an Arduino controller. The movement of the robot is controlled by a CNC-based Sinumerik numerical control unit. The control algorithm implemented in the system comprises a proportional-integral-derivative (PID) controller and the utilization of the Average Height Value (AHV). This combination ensures smooth movements and helps to avoid undesirable rapid movements that may cause issues during the printing process. To evaluate the effectiveness of the proposed method, a case study involving a circular structure with 50 layers and a radius of 250 mm is conducted. The results indicate that the proposed method successfully prevents earlier failures caused by irregular loading, thereby enhancing the stability and reliability of the printing process.

In addition of previous study, a real-time tool-path planning system was proposed by Yuan et al. to enhance system stability in 3D concrete printing (3DCP) processes [33]. The study reports that filament widths in 3DCP applications typically range from 6 to 50 mm, depending on the specific application. For larger-scale applications, wider filament widths are often utilized [34]. However, using wider filament widths can result in poor surface finish, rough details, and weaker components. Similarly, employing a constant filament width is not preferable as it can create structural weaknesses and lengthen printing times. To address this challenge, the study proposes a variable-width printing methodology that allows for simultaneous adjustment of the filament width during the printing process. The primary objective is to develop a system capable of printing components with variable cross-sections, reducing the overall tool path length, and consequently decreasing printing time. To achieve this, the researchers first selected a cement composition with quick shear stress gain to minimize the deformation effect, referring to relevant studies [35, 36]. Subsequently, a control system was developed, encompassing real-time sensor data acquisition, the generation of real-time tool paths, and the real-time control of print head movement. Process parameters including material flow rate (Q), nozzle speed (v), filament width (w), and layer height (h) were chosen for monitoring and control. The tool-path planning strategy utilized the Delaunay triangulation method within the cement extrusion system. The flow rate of extrusion was monitored by correlating motor speed with the amount of material passing through. This allowed for estimation of the flow rate based on motor speed. Real-time communication between the robot and the system was established using the FUrobot platform within Grasshopper. The tool center point (TCP) location was determined at 50 ms intervals using the aforementioned program. Communication between the robot and the sensor system was facilitated through the KUKA Robot Sensor Interface 4.0. For geometric inspection of the printed parts, 3D laser scanning was employed. In this system, filament width was controlled and altered by manipulating the flow rate value and tool path. The system was tested using various filament sizes ranging from 6 mm to 20 mm. Each sample was printed with 10 layers. To simplify the printing process, a closed-loop continuous tool path was designed. The system was also tested for both symmetrical and asymmetrical contours, which are commonly encountered in variable-width printing. The results of the study demonstrated significant improvement in horizontal accuracy through the use of feedback control methods. Moreover, the system exhibited higher efficiency in printing both simple and complex shapes. It is important to note that the proposed control strategies in the previous studies primarily tackle post-extrusion challenges, such as deformations and variable filament widths. However, it is essential to recognize that a substantial portion of the challenges in 3D concrete printing (3DCP) stems from internal variances within cement-based mixtures [13]. These internal variances contribute to pre-extrusion instabilities that can significantly impact the overall quality and structural integrity of the printed components. Therefore, in order to provide a comprehensive solution, it becomes imperative to address both pre-extrusion and post-extrusion instabilities.

In order to address the need for inline control mechanisms, researchers have proposed a system that integrates printing and material parameters to facilitate smooth extrusion processes [37]. The study emphasizes the importance of incorporating these parameters to achieve optimal extrusion outcomes. To accomplish this, the researchers developed a feed-forward control system that includes control parameters tuned based on prior knowledge of the material's thixotropic behavior. The key parameters identified in the study include print speed, layer height, and pump flow rate. The control method implemented in this study utilizes shear stress measurement to estimate the flow rate value, establishing a relationship between fluid behavior and a feedback value. The instantaneous shear rate is measured using a shear vane apparatus, while extrusion is facilitated through a screw pump system. Experimental data was collected during trials, recording both shear rate and flow rate. Subsequently, an algorithm was created using the collected data, enabling estimation and control of the flow rate value based on the measured shear stress value (specifically, the motor torque value that rotates the vane apparatus). An Arduino micro-controller and a digital-to-analog converter circuit were employed to control the flow rate of the system. However, it is important to note that during the development of the control algorithm, a single cement mixture with a fixed raw material ratio was utilized. The rheological behavior of cement is highly influenced by the ratio of its raw materials. Even slight changes in the material ratio can significantly impact its flow behavior and alter its response to applied shear. Therefore, it can be concluded that the proposed system may not fully account for the changing material behavior and its direct relation to the flow rate value when the material ratio is modified. In summary, the proposed control mechanisms effectively utilize shear stress measurement and motor torque to estimate and adjust the extrusion rate. However, it is crucial to consider the influence of varying material ratios on the flow behavior of cement, as these changes may render the established flow rate-shear rate relation invalid. Further research and development are necessary to address the challenges associated with changing material behavior and ensure accurate and reliable control of the flow rate in 3D concrete printing.

Building upon the previous study, several other researchers have also put forth continuous control techniques to evaluate the quality of extrusion in 3D concrete printing (3DCP) [38]. These studies highlight the lack of quality monitoring and inspection during the 3DCP processes. It is emphasized that an inline real-time quality monitoring system, capable of detecting material property variations and taking proactive measures prior to material deposition, is crucial to prevent potential system failures and ensure consistent extrusion. The study explores and discusses four different control techniques that were implemented and tested. The first technique focuses on utilizing the power consumption of the agitator motor to detect rheological variations in the system. By monitoring the power consumption rate, material viscosity can be predicted. In the second technique, extrusion pressure is selected as the primary feedback value. The extrusion pressure is closely related to the viscosity of the composition, allowing for the detection of internal variations. The third technique involves using the electrical resistivity of the fluid to estimate internal variations within the system. While electrical resistivity is commonly employed as an assessment criterion for long-term performance in hardened concrete [39, 40, 41], fewer studies have explored its influence on fresh mortar and concrete . The main objective of this study is to establish a correlation between electrical resistivity and the water content of the cement mixture, with the hypothesis that internal variations can be detected by analyzing this parameter. The fourth technique incorporates computer vision as a real-time extrusion monitoring tool. Top-view images of the extruded layer are captured and analyzed using an algorithm that measures the actual extruded layer width and compares it to the target width. Experimental studies are conducted to test these techniques using different cement mixes. To account for cement mix variations, seven mixtures with varying free water content ratios are created, assuming that free water ratio is a significant source of variation. These seven mixtures are then used to assess and evaluate the proposed control techniques. Overall, promising results are obtained with all techniques, with the computer-aided technique demonstrating the most reliable outcomes. The proposed control techniques' limitation, though, stems from their narrow focus on particular control parameters. It is important to recognize that internal variations that happen during cement extrusion can have an impact on a number of parameters at once. A thorough system that simultaneously controls all pertinent parameters is required to address the complex interplay between these parameters and effectively mitigate internal variations. The complexity of internal variations in cement extrusion, in other words, requires a comprehensive system that simultaneously controls all pertinent parameters, even though the proposed control techniques have shown promise in addressing specific control parameters. By taking a holistic approach, the system can efficiently detect and react to internal variations, improving extrusion quality, stabilizing the process, and facilitating the printing of 3D concrete.

In addition to that, several studies have focused on systems aimed at reducing the extrusion pressure for 3D concrete printing (3DCP) by controlling the applied shear value on the mixture through the application of vibration [42]. One such study investigates the increasing popularity of automation in construction, specifically examining 3DCP cement extrusion in pumping, extruding, and construction aspects [43, 44, 45, 46]. The necessity of active rheology control in 3DCP applications is introduced, as it is discovered that the material should possess adequate strength and stiffness to support its weight [47], and the bond strength between consecutive layers must be improved [48, 49]. Consequently, the rheological requirements of 3DCP during the pumping and extrusion process are investigated to understand the type of control strategy that should be implemented [50]. Subsequently, an investigation into common failure types of 3DCP applications, such as "strength-based failure" [44, 45, 46, 51, 52, 53] and buckling failure [45, 52, 54, 55], is conducted to provide a solution. Based on this investigation, it is concluded that active rheology control can resolve the aforementioned issues. Various approaches for active rheology modification, including vibration [56], chemical triggers [57], thermal control [58], magnetic field [59, 60], and microwaves [61], are discussed, and the approach suitable for 3DCP applications is examined. Vibration is ultimately selected since multiple studies have confirmed its effectiveness in reducing the yield stress and improving the extrudability of 3DCP applications [62, 63, 64]. Following that, an approach to characterize the vibrational effect on rheological parameters is investigated. The relation found by Basterfield et al. [65] is employed to establish a correlation and characterize the vibration effect on rheological parameters by measuring extrusion pressure. Subsequently, a test setup is created using the ram extrusion technique. To validate the idea, three cement mixtures with different sand mass percentages are prepared. An electric vibrator and a frequency controller are attached to the end of the extruder barrel. A load cell is integrated into the system to measure the extrusion force, which is later converted to extrusion pressure by dividing it by the related area. A data acquisition (DAQ) system is employed to record force and displacement data. The mean extrusion velocity is calculated using the piston-driving velocity, barrel area, and orifice area. All the data is then inputted into the relation found by Basterfield to determine the unknown rheological parameters. This methodology is utilized to control the variations in rheological parameters of cement during extrusion. Additionally, the vibration effect on build-ability and mechanical properties is investigated. Overall, promising results are obtained, and this approach has led to enhancements in the overall layer quality, with certain structures demonstrating increased durability over multiple layers. However, it should be noted that in existing studies, the vibration rate remained constant across different cement-based mixtures, and no proposed correlation exists between the shear rate value and the rheological behavior of the extruded cement-based mixture. Considering that cement-based mixtures exhibit unique material behavior, it is likely that vibrations act at different rates. Consequently, the flow rate, extrusion pressure, and other parameters may vary across different cement compositions, potentially leading to additional problems. Therefore, it would be preferable to develop a system capable of adapting itself according to the specific mortar type.

Similarly, there have been studies on controlling viscosity in polymer extrusion [66, 67]. One of these studies addresses the complexity and unpredictability of the extrusion process, emphasizing the importance of process control and monitoring for improved efficiency. The complexity arises from the nonlinear relationship between process inputs, such as screw speed, and outputs, such as flow rate. The study claims that variations in viscosity can lead to issues and instabilities, resulting in weaknesses and product failures. Consequently, a proposed solution is to develop a system capable of directly measuring viscosity to enhance product quality.

Various viscosity measurement techniques are explored in pursuit of this goal. One such technique is the side-stream rheometer, which estimates viscosity based on pressure drop measurements in the capillary tube. However, these instruments suffer from significant measurement lag due to the transit time in the side-stream. Another approach is the in-line rheometer, which also utilizes pressure drop measurements to estimate viscosity. It is found that this method yields better results; however, it has not been tested for control purposes. Consequently, researchers decide to investigate similar capillary-type rheometers and enhance the concept by introducing a feedback control system.

To facilitate their research, an experimental setup is constructed. This setup employs a gear pump to extract a continuous sample from the nozzle, while a wall-mounted transducer in the reservoir measures the pressure drop prior to the capillary die. An equation relating pressure, flow rate, and viscosity is used to estimate viscosity. The flow rate is determined by the mass flow rate set by the gear pump. Under controlled conditions such as temperature and material, several tests are conducted using the aforementioned approach. The estimated viscosity values are then compared with those obtained from laboratory measurement devices, yielding promising results with minor offset errors.

In the second study, the control mechanism is similar; however, it utilizes temperature to manipulate viscosity during the extrusion process. Nonetheless, in both studies, their working principles are not applicable to cement-based materials due to the potential introduction of chemical reactions and distortion of the cement. Furthermore, the model correlation in these studies is based on a single polymer composition, rendering them insufficient for handling different fluid compositions.

1.2 Scope, goals and significance of the thesis

Looking at the previous studies, while a continuous, universal, and automated quality assessment mechanism is essential to ensure the quality of cement extrusion, it is also crucial to incorporate rheological parameters for the effectiveness of such a control system [68]. However, despite the extensive research conducted, a comprehensive control system that can fulfill all the needs of the 3D concrete printing process has not yet been established.

To meet the needs of the industry, this thesis presents a comprehensive methodology and implementation approach for developing a flow rate control system to be utilized in 3D Concrete Printing (3DCP). The study encompasses multiple aspects, including material determination, data collection strategies, non-dimensional analysis of cement extrusion, implementation of the control method, test results of the implemented control method, and a thorough discussion of the obtained results.

The primary objective of this study is to demonstrate the integration of rheological properties of the material into the printing parameters of the extrusion process. By establishing this relationship, the study aims to pave the way for the development of new control strategies that can be derived from the established correlations.

The study incorporates various stages, starting with the identification and characterization of suitable materials for 3DCP. Data collection strategies are then devised to gather essential information on flow behavior and rheological properties of the selected materials.

Non-dimensional analysis techniques are applied to examine the cement extrusion process in a more generalized manner, allowing for the identification of key parameters and their impact on the printing process. This analysis provides valuable insights into the relationships between rheological properties and printing parameters.

Based on these findings, a flow rate control system is implemented and tested. The test results are thoroughly analyzed and discussed, considering the effectiveness and efficiency of the control method in regulating the flow rate during the 3DCP process.

This thesis is crucial in demonstrating how the integration of material rheological properties and printing parameters in the extrusion process can lead to the development of a universal control system for 3D concrete printing (3DCP) applications.

It lays the foundation for the development of new and improved control strategies, offering opportunities for further advancements in 3DCP technology.

The significance of the thesis can be listed as;

1. Using non-dimensional analysis to find dimensionless numbers governing an accurate relation between printing parameters and rheological properties.

2. Proposing a novel approach to estimate the instantaneous flow rate of the extrusion using pressure drop, demanded torque, and Herschel-Bulkey parameters of the material.

3. Proposing a control system for 3D Concrete Printing (3DCP) applications that can operate independently of the specific cement-mix design utilized within the system.

1.3 Thesis Structure

This thesis consists of the sections described below :

1. *Introduction*: The introduction section provides an overview of the background and context of the 3D cement printing process, as well as a review of relevant previous studies. It discusses the current status of 3D cement printing processes and highlights the challenges that arise during the operation of such systems. Additionally, the section investigates any existing literature gaps in the field. This section aims to establish the research goal of the study based on the findings from the literature review. By identifying the existing gaps and limitations in the field, the research goal is formulated to address these gaps and contribute to the advancement of 3D cement printing technology.

2. *Methodology* : The methodology section provides a detailed account of the progression of the study. It outlines the steps involved in the selection of dimensionless groups that will be utilized in the control method. These dimensionless groups serve as key parameters for understanding and regulating the 3D cement printing process. The rationale behind the selection of these groups is thoroughly explained.

   Furthermore, the section describes the simulation of the 3DCP process, which was conducted to gain insights into the behavior and dynamics of the printing process. The simulation results and observations are used to inform the design and setup of the experimental procedures.

The experimental setup, based on the insights gained from the simulation, is introduced in this section. The step-by-step process of the simulation is outlined, including the specific parameters and variables considered. This ensures transparency and replicability of the experimental procedure.

Moreover, the section delves into the experimental procedure for data collection. It provides a comprehensive explanation of the steps involved, highlighting the measurements and observations made during the experiments. The material selection for the experiments is also discussed, with considerations given to the rheological properties and suitability for the 3DCP process.

The flow rate control system is explained in detail within this section. Subsections are dedicated to different aspects of the control system, providing a thorough understanding of its design, implementation, and functionality.

3. *Experimental verification and discussion*: In this section, the findings obtained from the tests of the flow rate control system are presented, analyzed, and discussed in detail.

   The section begins by presenting the collected data and results from the experiments conducted using the flow rate control system. The data is presented in a clear and organized manner, allowing for easy interpretation and analysis.

   Following the presentation of the data, the results are analyzed using appropriate statistical and analytical methods. Key observations and trends are identified, and any significant findings are highlighted. The analysis aims to provide insights into the performance and effectiveness of the flow rate control system in regulating the flow during the 3DCP process.

4. *Conclusion*: The conclusion chapter serves as a summary of the findings and

major outcomes of the study. It provides a concise overview of the key results and their implications in the context of the research goal and objectives.

CHAPTER II

METHODOLOGY

This study focused on conducting a non-dimensional 3D cement printing process analysis. The first step involved identifying the parameters that influence the system. Subsequently, these parameters were combined in different ways to create a variety of non-dimensional groups. Following the creation of the non-dimensional groups, they were paired up to investigate the relationships between them. The main objective of the pairing process was to discover a non-dimensional pair that is highly correlated and can accurately depict the cement extrusion process. This non-dimensional pair would then be utilized to establish a control strategy for 3DCP processes. More information on this analysis is given in the following sections.

2.1 Dimensionless group selection

The non-dimensional analysis is a useful method for creating a valid mathematical model that can define the extrusion process. This technique removes the physical dimensions of the problem, providing an alternative perspective and making the model more universal, thereby increasing its applicability. This method is highly utilized in fluid-related problems. Instead of individually examining the variables that impact the system, this approach allows for testing a few key variables that carry the most essential information. Furthermore, since the non-dimensionalized problem lacks physical dimensions, it can be easily scaled up or down as required by the project. By employing predefined graphs representing non-dimensional groups, various types of projects can be established. To carry out such an analysis, the outlined steps should be followed below:

1. Determine all the parameters involved in the system. Let the number of selected parameters be denoted as n.

2. Select the primary dimensions based on the project requirements, such as temperature T, length L, time t, etc. The number of selected primary dimensions will be denoted as r.

3. Derive the dimensions of the selected parameters using the chosen primary dimensions.

4. Choose r parameters, including all the selected primary dimensions, from the list of parameters obtained in step 1.

5. Formulate equations, where each equation includes the parameters selected in step 4 and an additional parameter from step 1 that is different from the parameters in step 4. Multiply all the parameters together in each equation. The parameters selected in step 4 will have unknown power coefficients (e.g., a, b, c, etc.).

6. Determine the unknown coefficients that result in the overall dimension of the equation being 0. In total, $r - m$ equations will be formed, with each equation serving as a non-dimensional group.

A study on cement extrusion, which utilizes non-dimensional analysis as its basis, has been conducted due to the benefits offered by this approach. To utilize this method, parameters that are both measurable and effective in a cement extrusion were selected. These selected parameters are given in Table 1. Using these parameters, feasible dimensionless groups were established.

The procedure for conducting non-dimensional analysis involves the application of the Buckingham Pi Theorem, which is described as follows. In the case of cement extrusion, we consider the following important parameters: density (ρ), pressure (P), yield stress (τ), torque (T), flow rate (Q), angular velocity (ω), kinematic viscosity (ν), nozzle edge length (D), distance between pressure sensors (L), flow velocity (V), and dynamic viscosity (μ). These parameters amount to a total of 11, denoted as n (where $n = 11$). Table 1 provides a list of the selected parameters. To determine the dimensions of each parameter, the primary dimensions of mass (m), length (l), and time (t) are employed. The primary dimension count is represented by r (where $r = 3$). Among the 11 selected parameters, density (ρ), nozzle edge length (D), and fluid velocity (V) are chosen as primary variables.

Subsequently, equations are formulated in which each equation incorporates the primary variables and an additional parameter from the set of 11 parameters that differs from the primary variable. In each equation, all parameters are multiplied together, with the primary variables assigned unknown power coefficients a, b, and c, while the selected additional parameter has a power of 1. The aim is to determine the unknown coefficients that yield an overall equation dimension of 0. This process results in the formation of $n - r$ (8 in this case) equations, each of which represents a non-dimensional group.

To illustrate this procedure, an example is provided. In the first non-dimensional group, pressure (P) is chosen as the additional parameter, while density (ρ), nozzle edge length (D), and fluid velocity (V) are the primary variables. The equation to be solved is set as $\Pi_4 = \rho^a D^b V^c P$. The dimensions of the parameters are derived as follows: ρ has dimensions of mass per cubic length (M/L^3), D has dimensions of length (L), V has dimensions of length per time (L/t), and P has dimensions of mass per length squared per time squared ($M/(Lt^2)$). Three equations are then established using the above equation: $a + 1 = 0$, $-3a + b + c - 1 = 0$, and $-c - 2 = 0$. Solving these three equations yields the unknown coefficients $a = -1$, $b = 0$, and $c = -2$. Ultimately, the first non-dimensional group is determined to be $\Pi_4 = P/(\rho V^2)$.

Following a similar approach, all eight non-dimensional groups are formed. Additionally, by adhering to the rules of the Buckingham Pi Theorem, four more non-dimensional groups are created through mathematical operations involving the existing non-dimensional groups. The theorem allows for any mathematical operation that preserves the non-dimensionality of the equations. Consequently, a total of 12 non-dimensional groups are generated through this study. The generated dimensionless groups are given as :

$$\Pi_1 = \frac{\Delta P L^3}{T} \qquad \Pi_2 = \frac{\pi^2 \nu D^4 \omega}{Q^2}$$

$$\Pi_3 = \frac{\Delta P Q}{\omega T} \qquad \Pi_4 = \frac{\Delta P}{\rho V^2}$$

$$\Pi_5 = \frac{\tau}{\rho V^2} \qquad \Pi_6 = \frac{T}{\rho D^3 V^2}$$

$$\Pi_7 = \frac{Q}{D^2 V} \qquad \Pi_8 = \frac{D\omega}{V}$$

$$\Pi_9 = \frac{\nu}{VD} \qquad \Pi_{10} = \frac{\rho V D}{\mu}$$

$$\Pi_{11} = \frac{L}{D} \qquad \Pi_{12} = \frac{\tau T}{\rho^2 V^4 D^3}$$

Later, an experimental setup was designed to measure and record the related parameters. Data collected with this experimental system were used to analyze the relationships between dimensionless groups.

Table 1: Selected physical parameters of an extrusion system used in the non-dimensional analysis

Parameter	Unit	Dimension	Description
ρ: Density	kg/m^3	M/L^3	Measured density of the cement paste
D: Nozzle diameter	m	L	Equivalent diameter of the square cross-section extruder outlet
ΔP: Pressure drop	N/m^2	M/LT^2	Pressure difference between inlet and outlet pressure sensors
T: Torque	Nm	ML^2/T^2	Demanded torque of the DC motor rotating the extrusion screw
Q: Flow rate	m^3/s	L^3/T	The volume of cement per unit time measured at the extruder outlet
ν: Kinematic viscosity	m^2/s	L^2/T	Cement's internal resistance to flow under gravitational forces
L: Tube length	m	L	The distance between the two pressure sensors
ω: Angular velocity	rad/s	T^{-1}	Angular velocity of the extruder screw
μ : Dynamic viscosity	$kg/m.s$	M/LT	Measure of cement's resistance to flow
V : Flow velocity	m/s	L / T	The velocity of cement during flow
τ : Yield stress	N/m^2	M/LT^2	The required force to induce flow in cement

2.2 *Simulation of the 3DCP process*

Before proceeding with the actual experimental setup, the extrusion process of cement is thoroughly investigated through a series of simulation cases. The primary objective is to explore the potential relationships and interactions among the selected physical parameters in order to identify the most optimal parameters for the system. The findings obtained from these simulations serve as a basis for designing the test setup.

2.2.1 Model simulation

In preparation for the actual tests, a series of simulations are conducted using the Simcenter StarCCM+® computational fluid dynamics program to gain insights into the overall phenomenon.The screenshot in Figure 1 shows the program's scene window with a visible meshed part.

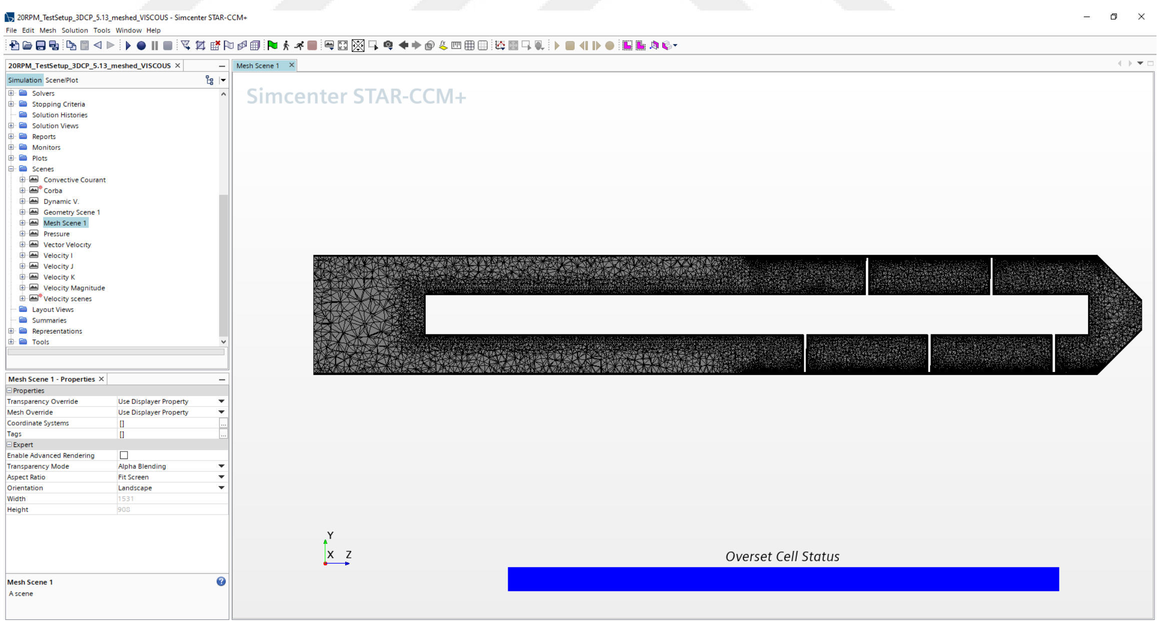

Figure 1: A screenshot from StarCCM+ displaying the meshed part of the cement extrusion system

The simulation environment consists of a simplified representation of the actual hardware while keeping the boundary conditions unchanged. The simulation comprises a screw and a cylindrical tube, representing a simplified version of the extrusion process. The barrel has a diameter of 110 mm, and the screw has a diameter of 105 mm, resulting in a clearance of 2.5 mm between them. Both parts have a length of 780 mm.

The solid surfaces, such as the screw surfaces and inner walls, are configured with no-slip wall boundary conditions, indicating that there is no relative motion between the fluid and these surfaces. The remaining boundaries, including inlets and outlets, are set as pressure outlets, allowing the cement to exit freely from the sides.

To facilitate separate treatment of each region, the fluid domain is divided into two regions within the simulation.

The initial region is referred to as the *Fixed Region*, where no rotation takes place. This region encompasses the inlet and outlet surfaces, as well as the walls of the tube. The second region, known as the *Rotating Region*, is where the primary interaction between cement and the screw occurs. This region is designed to include the fluid domain affected by the rotation of the screw. The program automatically establishes an interface between these two regions, enabling the computation of expressions across both regions.

To simulate the rotational effect, the *moving reference frame method* is employed. In this method, the *Fixed Region* is specified as stationary, while a new rotating reference frame is created for the *Rotating Region* along the z-axis direction. This allows for the effective representation of the motion within the *Rotating Region* while maintaining a stationary reference frame in the *Fixed Region*.

The *moving reference frame method* allows for the simulation of motion in a system without physically moving the screw itself. The region encompassing the screw, known as the *rotating region*, is then rotated by a specified value. As a result, the fluid flowing through the region affected by this motion interacts with the screw walls, causing deflections upon impact. This method effectively emulates the desired motion and is commonly employed in fluid dynamics programs. In the context of this project, the minor disparity between the actual rotation and the rotating region is insignificant, making the method suitable for its application.

2.2.2 Physical model selection and mesh operation

For the physical model selection, a viscous model of Generalized Newtonian fluid (GNF) is utilized, assuming a three-dimensional (3D), laminar, and steady flow condition. The gravitational force is considered in the "-z" direction.

The chosen non-Newtonian model is the "Generalized Power Law," which is a built-in model within the software. This model (referred to as equation 1) has been extensively studied in various studies [69, 70] and is known to provide faster results with sufficient accuracy.

The Generalized Power Law rheology model is a part of the GNF model and combines two rheology models, namely the Herschel-Bulkley and power-law models, into a more comprehensive formulation. The specific equation for this model is as follows:

$$\mu(\dot{\gamma}) = \begin{cases} \mu_0, & \text{if } \dot{\gamma} < \frac{\tau_0}{\mu_0} \\ \frac{\tau_0 + (\dot{\gamma} - \frac{\tau_0}{\mu_0})^n}{1}, & \text{if } \dot{\gamma} > \frac{\tau_0}{\mu_0} \end{cases} \tag{1}$$

where k is the viscosity index, n is the flow index, τ_0 is the yield stress threshold, μ_0 is the yielding viscosity and $\dot{\gamma}$ is the shear rate.

To verify the selected physical model, the dynamic viscosity vs shear rate plot (Figure 2) is created for cement samples. The orange points represent the rheological real data whereas the blue points represent the data gathered from the simulation program.To generate such a plot, cement samples are supplied to the rheology machine for processing. The rheology machine applies shear to the cement sample within a range of 0.1 to 100 shear rates, while measuring and calculating the shear rate. Subsequently, the program used for rheology machine control automatically calculates the corresponding dynamic viscosity for each shear rate. Next, a simulation is conducted, where the rheological parameters are selected to match those of the cement sample. The same shear effect is applied to the cement in the simulation, and the resulting dynamic viscosity value is recorded, as done previously. Finally, the values obtained from both the simulation and the rheology machine are plotted together to observe the correlation between them. Upon examining the plot, it is evident that the two curves align perfectly. This indicates that the chosen physical model is accurate and provides results that effectively represent the selected sample, with an acceptable margin of error.

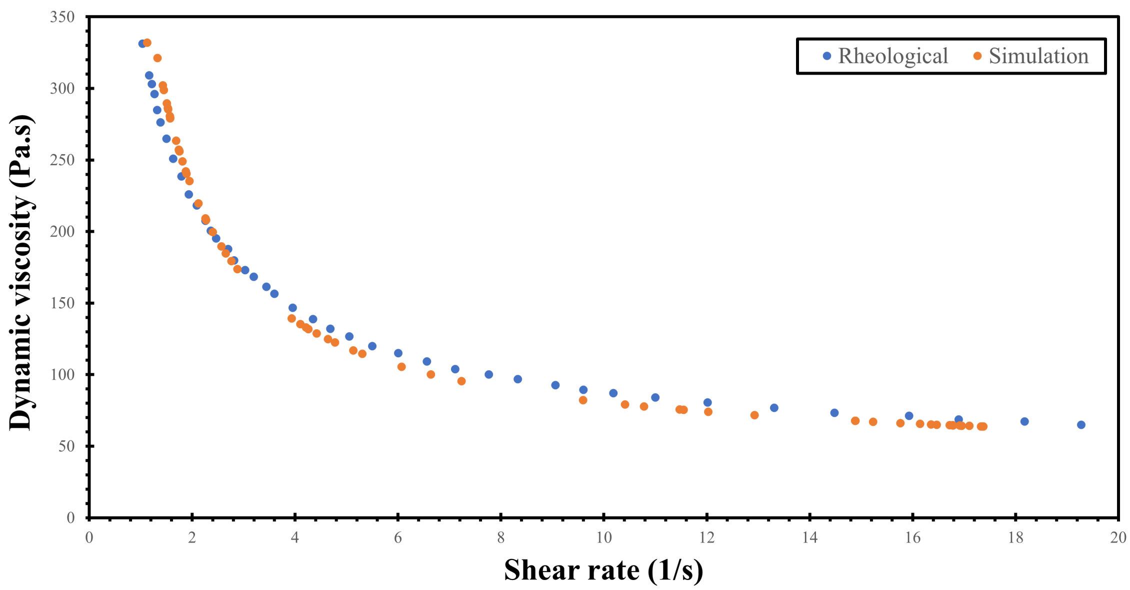

Figure 2: Dynamic viscosity vs shear rate analysis between rheological and simulation data for a cement sample. The orange points represent the rheological real data whereas the blue points represent the data gathered from the simulation program.

The meshing operation for this simulation is performed using an automated mesh tool, employing a tetrahedral mesh. Due to the requirement of the viscous model used in this simulation, tetrahedral meshing is the only viable option.

The base size of the mesh is set to 30 mm. To optimize the total mesh volume, surface, and volumetric controls are implemented. Surface controls are applied around the screw surface, while volumetric controls are defined in the rotating region. Both controls have a custom size of 10% relative to the base size. These controls help ensure an optimized mesh configuration in the critical areas of interest.

Overall, the simulation employs a mesh consisting of 433 thousand cells and 809 thousand faces, providing a suitable resolution for the analysis.

2.2.3 Data collection process and convergence criterion

After the selection and verification of the physical model, the main simulation for the methodology test is created. Data-gathering operations are conducted using various tools such as line probes, faces, and plots. These tools enable the collection of important parameters that play a crucial role in the cement extrusion process.

The following parameters are among those gathered:

Q: The flow rate of the cement.

ΔP: The pressure drop across the tube.

T: The torque value required for the extrusion process.

ν: The dynamic viscosity of the cement.

ω: The rotation rate of the screw.

These parameters provide essential insights and measurements during the simulation.

The geometric parameters in each simulation remain known and constant. The cylindrical tube radius is represented by R, and the distance between pressure sensors is denoted as L. The remaining parameters, such as the flow rate of the system (Q) and the pressure drop along the screw (ΔP), are calculated and monitored until steady conditions are achieved.

Figure 3 depicts the geometric scene of the simulation. In the given configuration, the plot illustrates the different regions and measurement points within the system. The light brown surfaces represent the inlet and outlet surfaces, which are set as pressure outlets, allowing fluid to freely enter and exit the system. The dark gray region represents the rotating region, which includes a screw and is responsible for inducing rotation. On the other hand, the light gray area represents the fixed region, where no additional rotation effect is applied, and the fluid moves freely. The purple surface serves as a measurement area where viscosity and pressure values are recorded. These recorded values help analyze variations across different samples. Specifically, a line probe is positioned between two pressure measurement points, acting as a data-gathering tool for capturing pressure and shear rate values. This enables the examination of how pressure and shear rate change within the system.

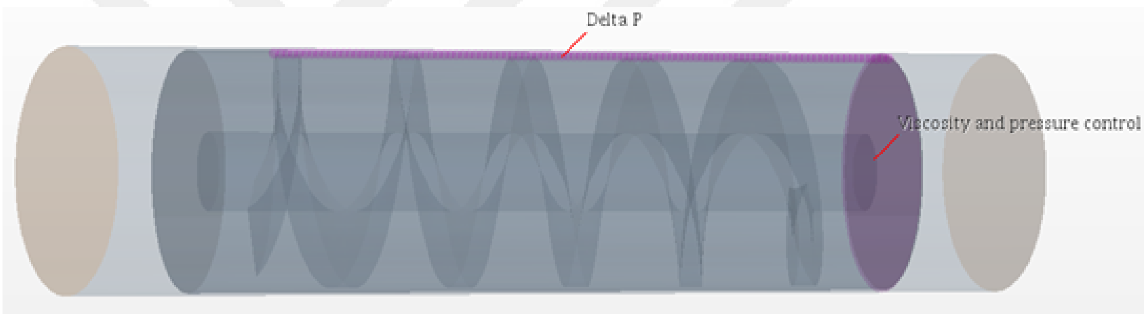

Figure 3: Geometric scene of the simulation

To determine simulation convergence, two criteria are utilized: residual error and inlet-outlet flow rate values. The simulation is considered converged when the residual errors for momentum in all directions and continuity reaches a sufficiently low value (typically below 10^{-4} for each parameter) and so the discrepancy between the inlet and outlet flow rates becomes insignificant. This ensures the conservation of mass and confirms the convergence of the simulation. The residual error report from a simulation result is given in Figure 4.

For each different cement sample, the flow rate Q and the pressure drop ΔP are recorded with varying rpm values which are changing +0.5 rpm for each run. The simulation is started at 0.5 rpm and the whole data-gathering procedure is repeated until 5 rpm is reached. This procedure is followed for each different cement sample and average velocity, average flow rate, ΔP, and real outlet dynamic viscosity are recorded.

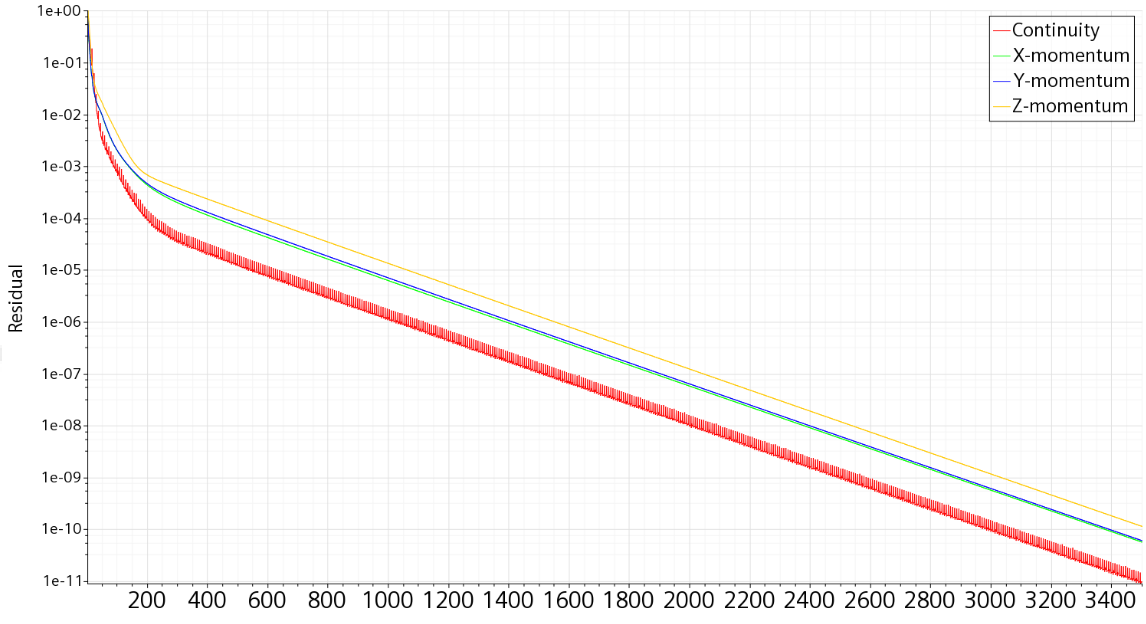

Figure 4: The change of residual error between each iteration for momentum and continuity equations during a simulation case

2.2.4 Simulation Analysis

Once the data is collected, the focus shifts toward investigating the cement extrusion process. The primary goal is to develop an intuition and gain a deeper understanding of the nature of cement extrusion. This involves examining the printing parameters involved in the process and, more importantly, analyzing the role and impact of the rheological characteristics of the cement samples on the overall process. This investigation helps in comprehending the behavior of the cement during extrusion and provides valuable information for process optimization and control.

One notable observation is that the flow rate values vary significantly across different cement samples, even under identical rotational rate conditions. The flow rate value indicates the volumetric amount of the extruded cement per second from the nozzle. This finding emphasizes the fact that when the composition of the cement sample is altered, the corresponding flow rate extracted from the system also undergoes substantial changes. Therefore, continuous monitoring and control of the flow rate is crucial in order to address and mitigate over-filling and under-filling issues that may arise as a result of these variations. The substantial variation in flow rate values highlights the importance of closely monitoring the flow rate during the cement extrusion process. By doing so, any deviations or fluctuations can be detected and addressed promptly, ensuring the stability and accuracy of the extrusion process.

Another important observation is the significant variation in torque and pressure values arises due to screw rotation across different cement samples. Here torque value indicates the necessary power which should be supplied to the motor to turn the extrusion screw and the pressure value represents the force applied to the inner walls of the extrusion tube from the fluid due to internal motion and related dynamic effects. This finding suggests that the torque value can be utilized as a feedback parameter from the system. This feedback parameter can be further analyzed and potentially incorporated into a control system. By monitoring and analyzing the torque values during the extrusion process, valuable information can be obtained regarding the behavior and characteristics of the cement samples. This data can serve as a feedback signal, allowing for real-time adjustments and control of the extrusion system.

The aforementioned observations can also be extended to the internal pressure fluctuations within the system. Figure 5 visually presents the pressure variations across different cement samples, all subjected to identical extrusion conditions. Each line in the plot represents the difference between the inlet and outlet pressure values for different cement compositions, each having distinct rheological properties. To generate this plot, a total of 10 different cement samples are selected. Subsequently, 10 simulations are conducted for each sample, with rotation rates ranging from 0.5 to

5 rpm. The simulations continue until convergence is achieved, indicated by satisfying the convergence criteria. During the simulations, the pressure difference between the inlet and outlet surfaces is recorded. By plotting all the obtained simulation data together, the effect of rheological variations on the pressure drop value can be observed. Upon analyzing this figure, it becomes evident that despite the uniform rotational speed of the extrusion screw, there are notable variations in pressure values. The changes in the rheological parameters have a significant impact on the resulting pressure drop within the system. These variations are particularly prominent across different cement samples. Consequently, these observed variations can serve as valuable feedback signals for further analysis and optimization purposes.

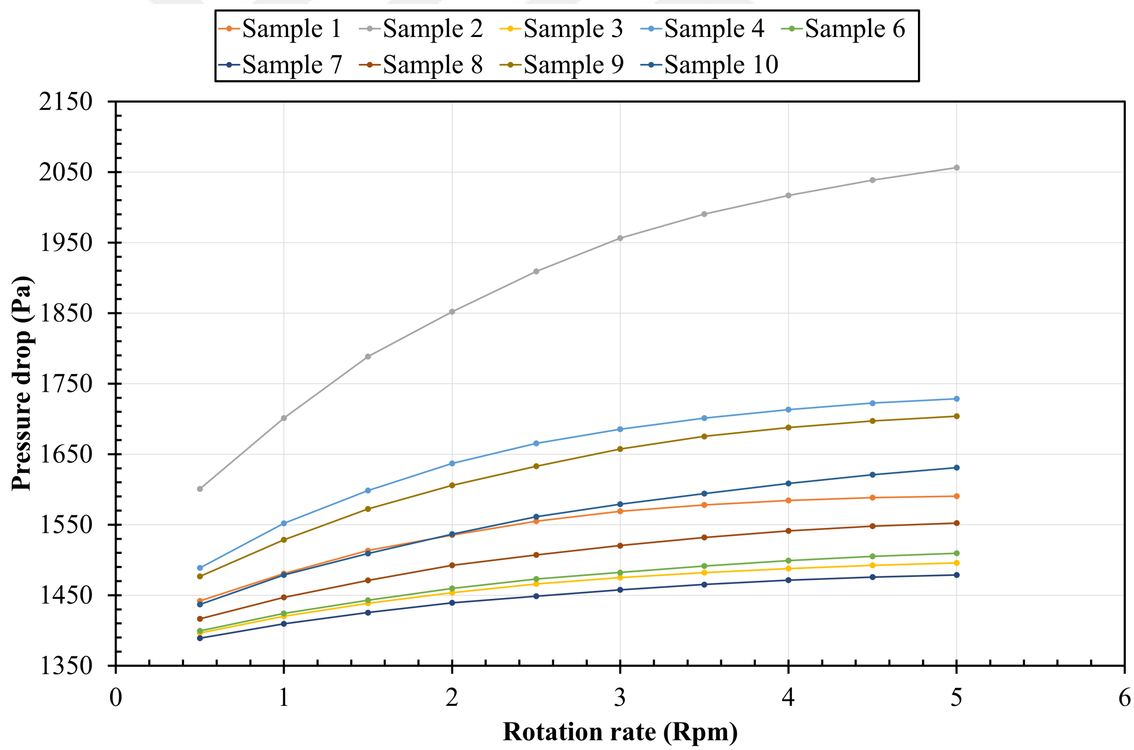

Figure 5: The plot shows the pressure drop across the tube during cement extrusion for different cement types and rotation rates. The x-axis represents the rotation rate of the extrusion screw, while the y-axis displays the pressure difference between upper and lower pressure sensors located near the system's inlet and outlet. Each line on the plot represents data collected from a different cement test and is colored differently for distinction.

An important discovery pertains to the variability observed in the outlet viscosity of the cement samples. This outlet viscosity holds significant influence over the flow behavior of the cement during the extrusion process, and it has the potential to impact the durability of the resulting extruded layer. The outlet viscosity value is closely linked to the flow characteristics exhibited by the cement samples, indicating how easily or resistantly the cement flows through the extrusion system. Figure 6 displays the outlet dynamic viscosity of different cement samples under identical printing conditions. Each line on the graph represents a cement mixture with distinct rheological properties. During the simulations, the outlet viscosities of the samples (i.e., the dynamic viscosity measured at the outlet nozzle during extrusion) are collected at various extrusion rates. For each cement sample, a simulation is performed with a predetermined rotation rate. The simulation continues until convergence is achieved, as denoted by satisfying convergence criteria. Once convergence is reached, the average dynamic viscosity at the outlet surface is recorded. Subsequently, the simulation is restarted with a different rotation rate, ranging from 0.5 to 5 rpm, for each cement sample. This process is repeated, resulting in the recording of pressure variation data for ten different cases for each cement sample. The collected data is thoroughly examined to gain insights into the parameters that significantly impact the outlet viscosity. Furthermore, the reasons behind the observed differences across the various cement samples are discussed, allowing for a deeper understanding of the underlying factors affecting the outlet viscosity.

After analyzing the collected data it is found out that the yield stress value of the cement sample is identified as a highly important factor in determining the outlet viscosity. A higher yield stress value is associated with a higher outlet viscosity. The continuous shear applied by the screw in the system plays a role in reducing the viscosity and facilitating flow. However, the initial yield stress value of the cement sample has a dominant influence on the overall outlet viscosity. Higher initial

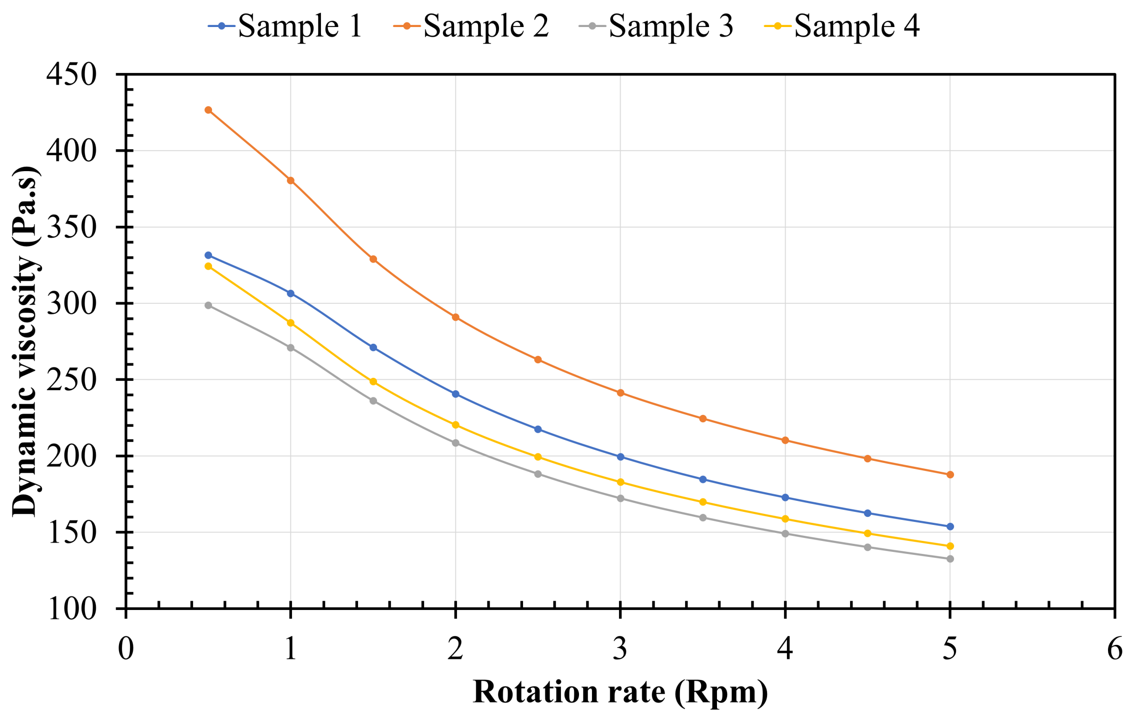

Figure 6: The plot illustrates the variation in dynamic viscosity during cement extrusion for different cement types and rotation rates. The x-axis represents the rotation rate of the extrusion screw, while the y-axis displays the dynamic viscosity of the cement. Each colored line corresponds to data collected from a distinct cement test.

yield stress values result in higher outlet viscosities, indicating a more resistant flow behavior.

Understanding the relationship between the yield stress value, outlet viscosity, and flow behavior of the cement samples is crucial for optimizing the extrusion process and ensuring the desired durability of the extruded layers. By carefully controlling the yield stress and managing the outlet viscosity, the flow characteristics of the cement can be manipulated to achieve the desired extrusion outcomes.

After the simulation analysis, an experimental setup is designed to gather data, taking into consideration important flow parameters such as flow rate (Q), pressure drop (ΔP), torque (T), and rheological parameters. The experimental system is carefully designed to enable continuous recording of these values.

In this setup, appropriate sensors and instruments are employed to measure and record the flow rate, pressure drop, and torque values continuously throughout the experiment. These sensors are carefully calibrated to ensure accurate and reliable data collection.

Additionally, specific equipment and techniques are employed to measure and characterize the rheological parameters of the cement samples. These may include rheometers or viscometers capable of providing precise measurements of viscosity, shear stress, and other rheological properties.

2.3 Experimental setup

To take advantage of the benefits of screw pump extrusion in 3D concrete printing (3DCP), including its capability for continuous material feeding, its common usage in material testing and optimization [71] and its potential for reducing the risk of consolidation [72], a screw pump system was incorporated into the experimental setup. The system setup is depicted in Figure 7. The left-hand side of the figure illustrates the developed test setup, while the right-hand side displays a CAD (Computer-Aided Design) representation of the step, indicated by arrows pointing to the labeled parts.

The experimental setup consists of a plexi-glass tube with a 100 mm diameter with 2 mm wall thickness. This material is strong enough to withstand stresses caused by extrusion pressure and also provides a visual advantage. The screw diameter is designed to minimize the gap between the outer screw wall and the tube to prevent any back-flow during extrusion. According to the research on screw designs [73], it has been found that screws with constant pitch length are the most effective for this system because these screws are not only simple in design but also has the highest throughput compared to other screws designs available. Therefore, a screw with a constant pitch (p=50 mm) length has been chosen for the system. The screw itself is custom manufactured from stainless steel to avoid any surface flaws due to corrosion.

In order to measure the pressure drop, the system includes 2 pressure sensors.

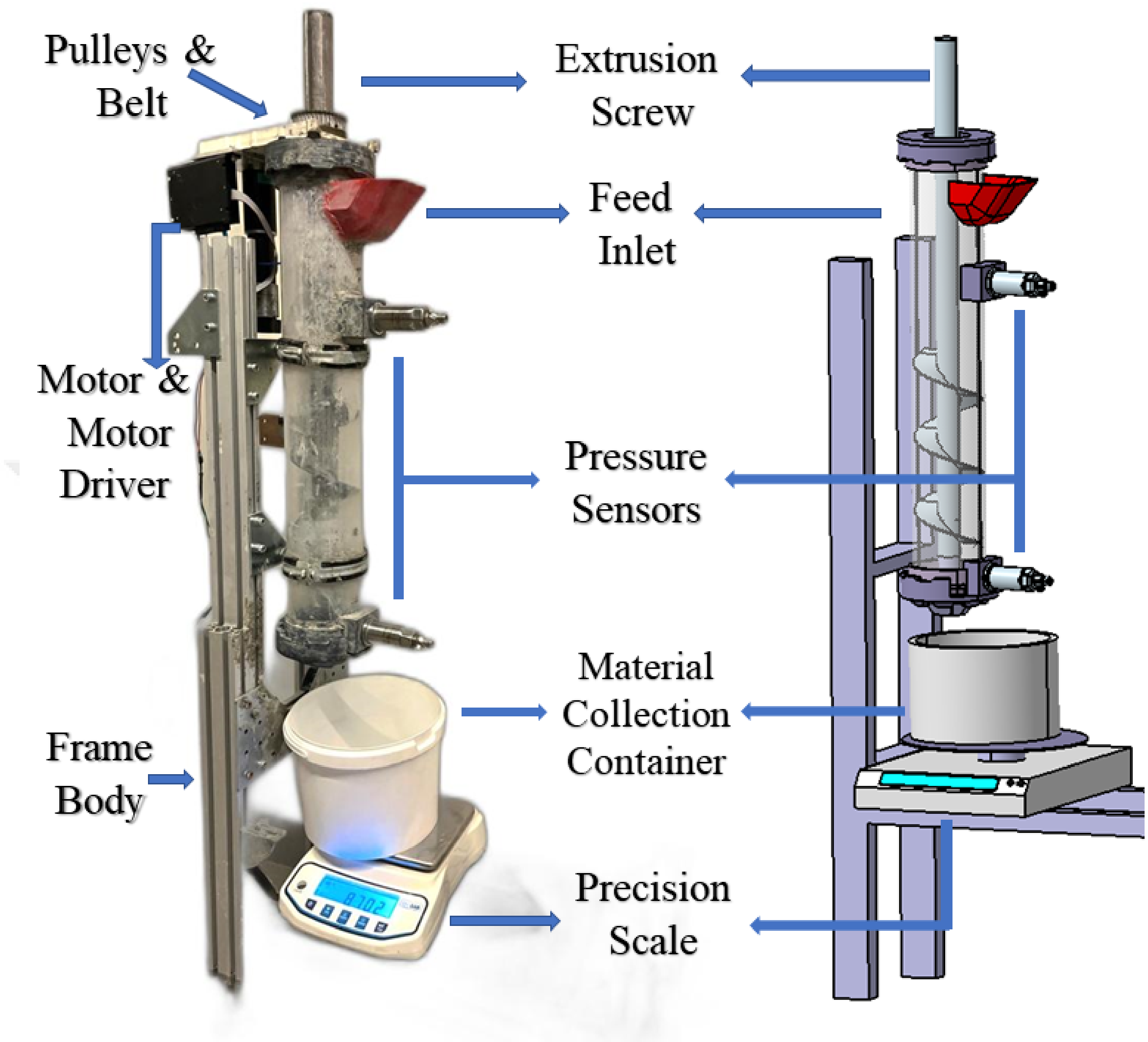

Figure 7: The overview of the cement extrusion setup. *Left*: Test setup, *Right*: CAD of the setup

Two front-flush type (IFM PM1689-PM1708) sensors with ceramic diaphragms were selected, so that the sensors would exposed to minimum damage from cement ingredients. The sensors can measure up to 25 kPa with a resolution of 0.01 kPa. These sensors are placed at the inlet and the outlet of the tube to measure pressure drop. Other fittings were created using 3D CAD software and manufactured from ABS material via 3D printing.

The experimental devices and their connections are shown in Figure 8. The DC

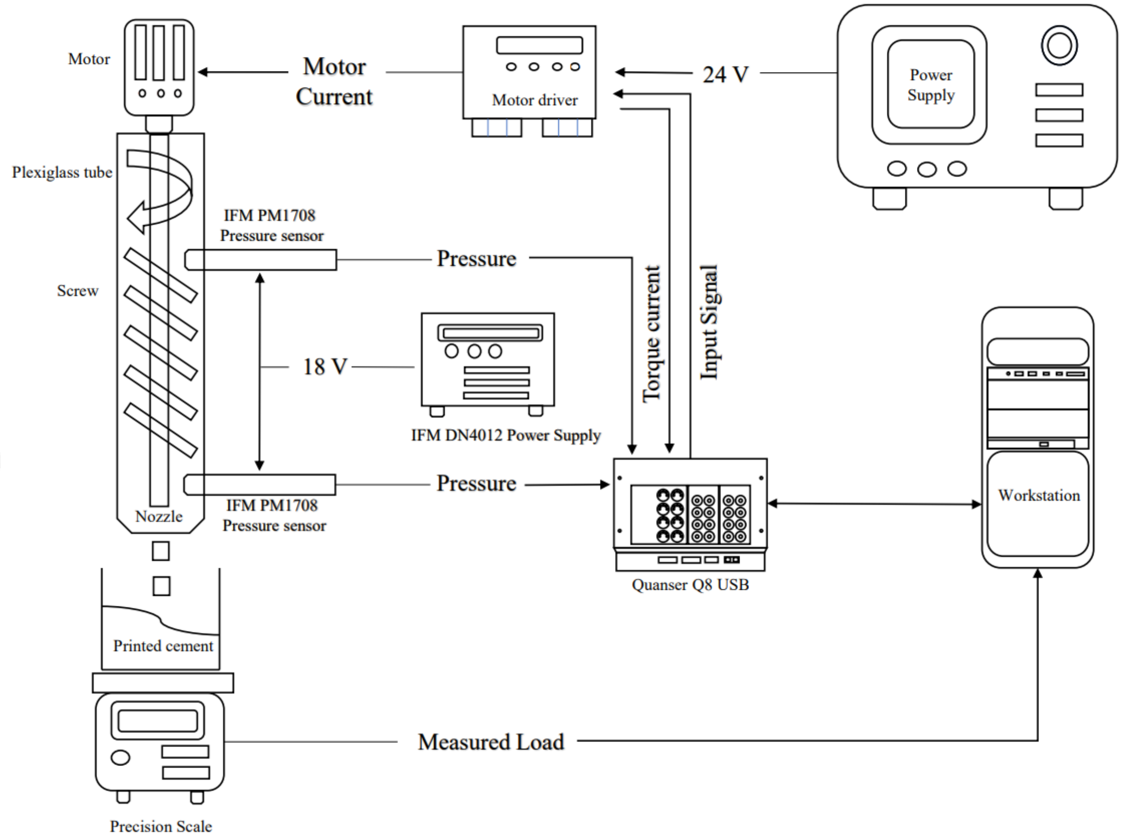

Figure 8: Technical representation of the test setup

motor is used to supply the torque required for extrusion and is linked to the extrusion screw with pulleys and a belt. The Maxon's Escon 50/5 servo driver is used to power the motor, and 24V DC supply is provided by the power supply. Motion control signals for the rotation are provided by the Quanser Q8 USB-type DAQ system, integrated with MATLAB Simulink, capable of generating 16-bit analog output control signals. The pressure sensors are also connected to the DAQ system to capture analog sensor data in real-time. A digital scale with a resolution of 0.01 g was used to measure the extruded sample (ISOLAB LS-EJ-3200AS). The data obtained during the measurements are saved on the workstation. The features of the experimental system are given in Table 2.

Table 2: Properties and specifications of the experimental setup

Feature	**Description**	**Unit**	**Value**
Nozzle size	Size of the nozzle through which cement extruded	mm	24
Extrusion screw	Part used to push material through extrusion pipe	-	stainless-steeel
Extrusion screw pitch	Distance between adjacent threads of the extrusion screw	mm	50
Motor stall torque	Maximum torque value can be supplied from the motor	mNm	931
Screw speed	Maximum rotational speed of the screw	rpm	15
Gear Ratio	Combined gear ratio of the motor gearbox and belt-pulley	-	1:319
Power supply voltage	Voltage required to operate both motor driver and pressure sensors	V	24
Tube diameter	Diameter of Plexiglass extrusion tube	mm	100
Pressure sensor measuring range	Operating range of pressure sensors	bar	-0.005 ... 0.1
Pressure sensor resolution	Smallest change in pressure that the sensor can detect and measure accurately	mbar	0.05
Internal volume	cement volume capacity	cm^3	≈3650

2.4 Material selection and analysis

The samples were prepared with Ordinary Portland Cement (OPC) CEM I 42.5 R and F-type fly ash (FA). The material characterization was previously given in the study [74]. The cement paste samples were prepared by water to a binder ratio (w/b) of 0.34. A viscosity-modifying agent (VMA) was used to modify the rheology of the mixes (0.3% of binder weight). Cement paste samples were prepared according to ASTM C305-14 Standard Practice for Mechanical Mixing of Hydraulic Cement Pastes and Mortars. However, a 100 L pan-type mortar mixer. Four mix designs were repared by varying FA replacement of 25, 30, 35, and 40% by cement weight. Rheological experiments were conducted by a commercial rotational rheometer (Anton Paar Rheolab QC) with a vane and container geometry. The flow curve of cement paste samples was obtained by applying a controlled shear rate flow curve (CSR) test protocol. A pre-shear was applied at a constant shear rate (300 s^{-1}) for 60 seconds. Following the samples were kept at rest for 5 minutes to enable the stabilization of the mixture after the high-shear pre-shear stage. Then, the shear rate increased from 0 s^{-1} to 100 s^{-1} in 60 seconds (up-curve) and decreased to 0 s^{-1} from 100 s^{-1} in 60 seconds (down-curve). The evaluation was done by using the down curve from each interval. The data obtained from the analysis was evaluated by the Herschel and Bulkley (H-B) model, shown in Eq. (2).

$$\tau = \tau_0 + k(\dot{\gamma})^n \tag{2}$$

where τ_0 is the dynamic yield stress (Pa), k is the viscosity index (Pa·s), and $\dot{\gamma}$ is the shear rate (s^{-1}). The index parameter n indicates the flow index of the material where $n<1$ for a shear-thinning behavior and $n>1$ for a shear-thickening behavior [75].

In order to select the appropriate material for the extrusion process, various mix designs are tested to identify a mixture with a prolonged setting time. These proposed mixtures undergo a series of test trials, each lasting approximately 1 hour. The objective of these trials is to assess the Herschel-Bulkley parameters of the mixtures and determine if they exhibit significant variations over time.

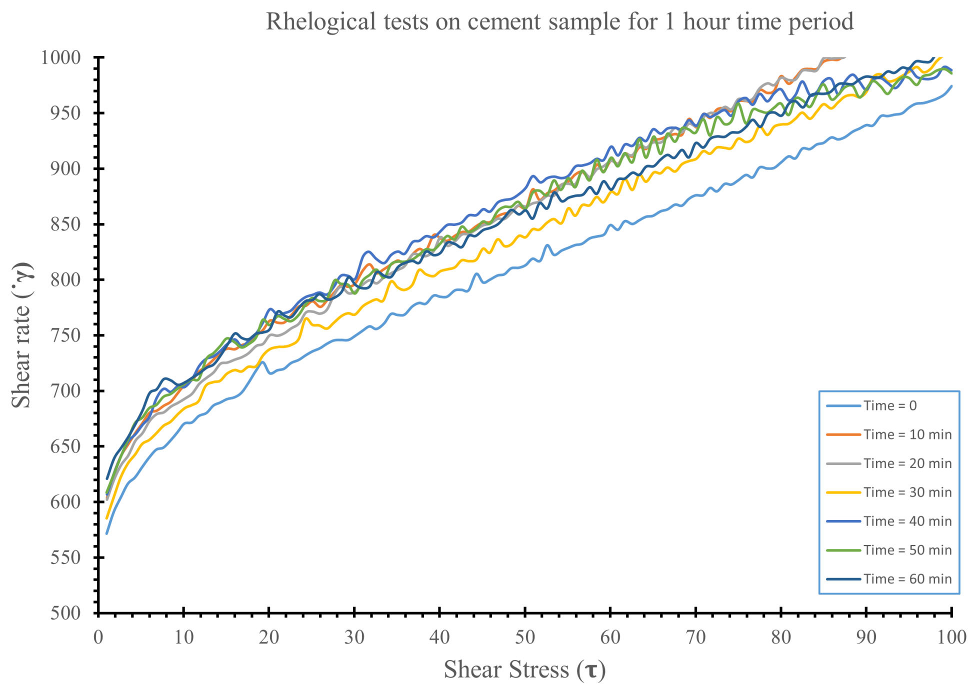

Figure 9: Shear stress vs shear rate plot of cement sample from 0 to 60 minutes

Upon analyzing the test data, it is observed that the Herschel-Bulkley parameters do not exhibit substantial differences within the given 1-hour duration. Figure 9 displays a set of test data, where each line on the plot represents a different time period ranging from 0 to 60 minutes. To generate this plot, a cement sample is selected and supplied to the rheology machine. The shear rate versus shear stress values are then recorded at different time intervals, starting from 0 minutes and progressing up to 60 minutes, with a 10-minute difference for each case. All the collected data is then plotted together to examine the impact of time on the behavior of the cement sample. This plot allows for the observation of how the shear rate and shear stress values change over time, providing insights into the time-dependent characteristics of the cement sample. Notably, the data lines coincide with one another, indicating consistent behavior across various time periods. Based on these findings, it can be concluded that each cement mixture can be used continuously for up to one hour without significant changes in its behavioral characteristics. This outcome provides assurance that the selected cement mixtures will maintain their stability and consistency throughout the duration of the experiment. The assumption simplifies the experimental setup and allows for a more straightforward analysis and interpretation of the results.

2.5 The test procedure and data collection

Experiments were conducted to collect data of the printing parameters such as pressure drop, ΔP , motor speed, ω, demanded torque, T, mass flow rate, Q, and rheological properties of the material, ρ, v, τ, k, and n. During these experiments, Herschel-Bulkley parameters of the material were assumed to be constant. An experimental procedure was established to preserve the repeatability of the data. Thus, the consistency of the experiments performed at different times was ensured.

The experimental guideline is given below:

2.5.1 Preparation and Calibration

1. Using the established recipe cement paste was prepared using a mixer

2. A small portion of the paste was used for the rheology test to get the shear rate, viscosity, shear stress, and torque values using the AntonPaar Rheolab QC rheology machine. These measurements were used to find Herschel-Bulkley parameters

3. A portion of the paste was used for density measurement

4. The remaining cement paste is used to fill the extrusion tube

2.5.2 Experiment

1. The cement paste was extruded with a determined speed (motor rpm, ω) to an empty bucket while recording the elapsed time. This operation was repeated for different time periods (30 s, 60 s, 75 s, 90 s) to determine the consistency of the extrusion process. The system was continuously supplied with the cement during each trial.

2. The torque and pressure values are recorded during the extrusion process.

3. The weight of extruded material was measured and with elapsed time knowledge

4. The test setup was filled again and the procedure was repeated. Before each loading, pre-shear was applied to the cement paste via a hand-mixer to establish homogeneity

2.5.3 Post-process

1. The flow rate, a vital metric in the process, is then calculated by dividing the weight of the extrudate by the elapsed time.

2. The gathered data is subsequently utilized to explore the relationship between non-dimensional groups.

Figure 10 depicts the flow diagram of the experimental procedure.

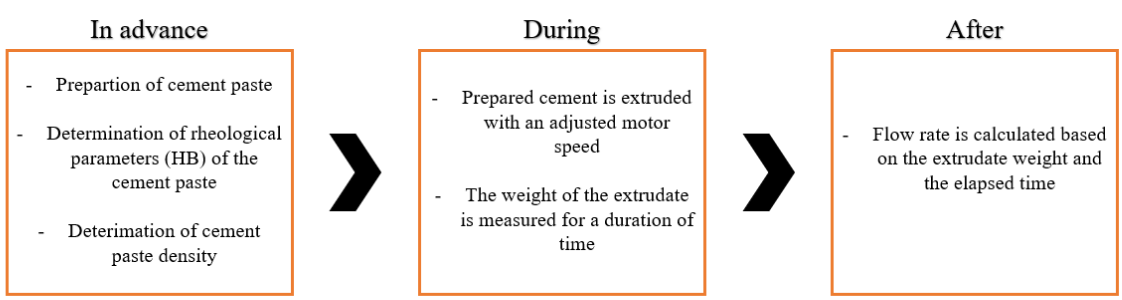

Figure 10: The flow diagram of the experimental procedure

2.6 Correlation investigation of non-dimensional pair

Using the specified experimental setup and approach, different datasets were collected by varying the extrusion rates and using various cement types with varying rheological parameters. Using the collected data, the non-dimensional groups were paired and analyzed for their relationship using curve fitting with various relation types.

The pairing process carefully ensures that the final equation includes all important factors, like pressure, torque, flow rate, and a rheological parameter. In this system, Π_7 and Π_{11} remain constant due to unchanged nozzle diameter D and tube length L throughout the tests. Therefore, both non-dimensional groups are excluded from the analysis. Furthermore, to avoid redundancy in correlation investigation, dimensionless groups with the same parameter are not pitted against each other. Instead, non-dimensional groups with distinct parameters are paired together. Through this process, eight eligible non-dimensional pairs are identified.

Subsequently, the correlation between these pairs is explored using different regression equations which are listed below:

i) Linear regression: This regression type relates the given parameters in a linear manner, given with the equation;

$$y = a \cdot x + b \tag{3}$$

where x is the dependent variable which is tried to be predicted and y is the independent variable which is used to predict the dependent variable. The constants a, and b are the regression constants.

ii) Polynomial regression: This regression type is used to describe the non-linear relationship between. Note that to prevent over-fitting the curve to the training data, a maximum polynomial order of 2 is set for the polynomial curve fit.

$$y = a \cdot x^2 + b \cdot x + c \tag{4}$$

where x is the dependent variable and y is the independent variable. The constants a, and b depicts the relation between x and y while constant c gives the random error.

iii) Power regression: This is another non-linear regression model which is specifically utilized for cases characterized by a gradual change at the beginning, followed by a rapid change over time. This regression uses the equation;

$$y = a \cdot x^b \tag{5}$$

where x is the dependent variable and y is the independent variable. The constants a, and b shows the nonlinear relation between dependent and independent variable.

iv) Logarithmic regression: This regression technique stands in contrast to power regression model. It is applied when the data exhibit a swift change at the outset, followed by a gradual decrease as time progresses. This regression type uses the equation;

$$y = a \cdot ln(x) - b \tag{6}$$

where x is the dependent variable and y is the independent variable. The constant a shows the relation between x and y while b is the offset error.

The goodness of fit measures, denoted by R^2, are presented in Table 3 for all four fit types. Also, the plot 11 gives a solution of an example curve fitting operation held on Π_1 and Π_2.

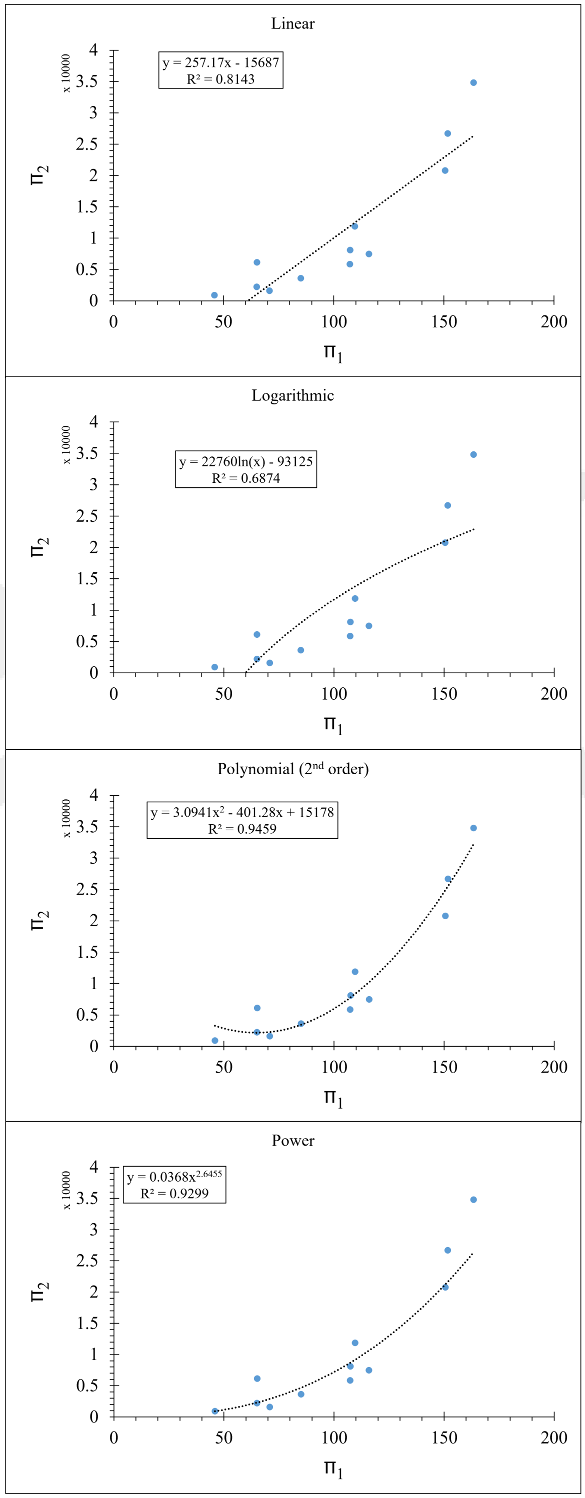

Figure 11: The plots of all 4 regression techniques applied on non-dimensional pair Π_1 and Π_2. Same for all plots, the x-axis shows the values of Π_1 while the y-axis shows the values for Π_2. The obtained equations for each regression model are given in the trend-line label. Blue dots display the data collected during the experimental trials. Each dot represents the mean value of an average of 6 test trials.

At the end of this procedure, it is found that the best correlation is achieved between Π_1 and Π_2 with a 2^{nd} order polynomial relation. To further improve the correlation score, different relationships are examined within the selected pair, for instance, comparing ${\Pi_1}^2$ against Π_2. Since both pairs are dimensionless, any mathematical operation preserving their dimensionless nature is considered valid. Consequently, taking different powers of dimensionless numbers is a viable approach. Ultimately, the best correlation is achieved between the dimensionless number pair, resulting in an impressive goodness of fit with $R^2 = 0.96$ for ${\Pi_1}^2$ versus Π_2. The plot that shows the relation between the pair is given in Figure 12. Further discussion on the selected pair is given below.

Table 3: The goodness of fit scores (R^2) of selected non-dimensional pairs for various regression strategies. The collected scores were used to investigate the relationship between pairs.

Non-Dimensional Pairs	**Linear**	**Quadratic**	**Logarithmic**	**Power**
Π_1 - Π_2	0.81	**0.94**	0.69	0.93
Π_1 - Π_5	0.69	0.72	0.62	0.72
Π_1 - Π_9	0.67	0.70	0.60	0.70
Π_1 - Π_{10}	0.59	0.74	0.69	0.82
Π_1 - Π_{12}	0.86	0.91	0.77	0.89
Π_3 - Π_5	0.58	0.59	0.54	0.6
Π_3 - Π_9	0.59	0.61	0.55	0.61
Π_3 - Π_{10}	0.45	0.72	0.56	0.78

The correlated non-dimensional pair is given in (7).

$$\Pi_1 = \frac{\Delta P\ L^3}{T} \quad \text{and} \quad \Pi_2 = \frac{\pi^2 \nu\ D^4 \omega}{Q^2} \tag{7}$$

Upon examining the selected non-dimensional pair, it was determined that only two parameters were suitable for selection as the control parameter: flow rate (Q) and kinematic viscosity (ν). After evaluating the advantages of each option, flow rate control was chosen as the preferred control parameter for the cement extrusion process. The primary reason for this decision is that flow rate control can help minimize the impact of drainage and ensure consistent extrusion, which are crucial factors for achieving successful cement extrusion [68]. Additionally, measuring the flow rate of the extrusion is relatively easy compared to measuring kinematic viscosity, making it a more practical and convenient option for the control system. Thus, based on these reasons, flow rate Q was selected as the primary control parameter for the cement extrusion process.

Due to the variable nature of kinematic viscosity in cement extrusion processes and the limitation of the proposed experimental setup in providing continuous measurement of this parameter, it is necessary to rewrite the kinematic viscosity in terms of other known or measurable parameters. The kinematic viscosity of the cement paste can be found using measured density value using (8).

$$\nu = \frac{\mu}{\rho} \tag{8}$$

where μ is the effective viscosity. The effective viscosity can be determined by dividing the average shear stress with the measured average shear rate as:

$$\mu = \frac{\tau}{\dot{\gamma}} \tag{9}$$

where $\dot{\gamma}$ is average shear rate and τ is the effective shear stress. The effective shear rate of the system is calculated using (10).

$$\dot{\gamma} = \frac{Q}{DA} = \frac{Q}{D^3} \tag{10}$$

The average shear stress on the system can be calculated using the Herschel-Bulkley equation using the recorded rheology parameters as in Equation 2.

After combining equations (2) through (10), the kinematic viscosity with the measured parameters is given in (11).

$$\nu = \frac{D^3(k(\frac{Q}{D^3})^n + \tau_0)}{\rho Q} \tag{11}$$

With the derived equation, all parameters of the kinematic viscosity can be measured or calculated. The second non-dimensional group, Π_2, given in (7) can be rewritten using (11) as:

$$\Pi_2 = \frac{\pi^2 D^7 \omega (k(\frac{Q}{D^3})^n + \tau_0)}{\rho Q^3} \qquad (12)$$

During each test session, various cement pastes with different rheological properties were utilized. For each test, a specific rotation rate is chosen. The cement sample is extruded at this rotation rate while recording torque, pressure, and flow rate. Subsequently, the system is restarted with either the same or a different rotation rate. In total, approximately six different cases are recorded for each cement sample. Later, non-dimensional group pairs are calculated using the average measurement values from these six repetitions. Figure 12 displays the data points of the non-dimensional group pairs obtained for each test session. Abscissa shows the square of Π_1 while the ordinate represents Π_2.

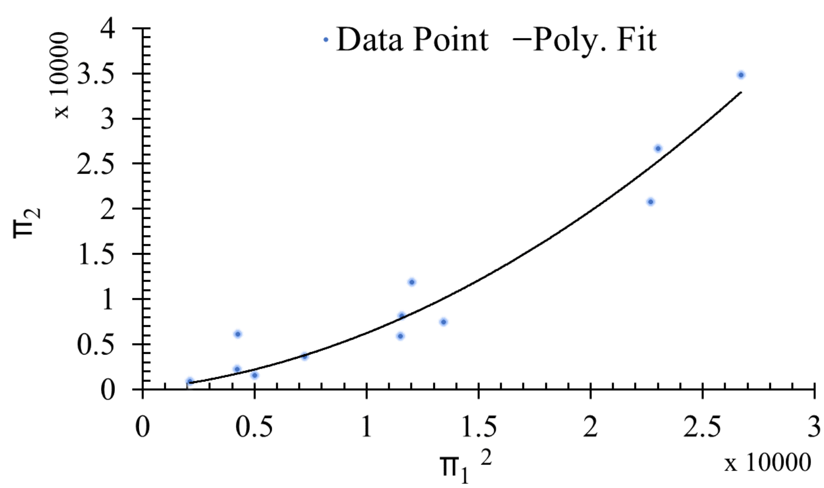

Figure 12: Second order polynomial relationship between Π_1^2 and Π_2 non-dimensional groups. Blue dots represent the average value of approximately 6 different test results. The black curve depicts the 2nd order polynomial fit between the non-dimensional groups. ($R^2 = .96$ the goodness of fit measure)

The correlation between the non-dimensional group pairs, which is represented by a second-order polynomial fit is given in (13).

$$\Pi_2 = 4 \cdot 10^{-5} \Pi_1^4 + 0.2608 \cdot \Pi_1^2 \tag{13}$$

In summary, this relation represents a comprehensive solution that includes both printing speed and material properties. Given the wide range of rheological and mechanical parameters represented in the data such as the variation of τ between 260-580 Pa, n between 0.4-0.8, and ω between 1-3 rpm, the model solution can be considered universal for the system. Also, the contribution of hydrostatic pressure resulting from the pressure sensors' position is intentionally disregarded, focusing solely on observing the pressure effect generated by the flow.

2.7 Numeric solution of Q for quality control

The correlation equation given in (13) can be also written as (14) using known or measurable parameters and correlation constants a, b.

$$\underbrace{\frac{\pi^2 D^7 \omega (k(\frac{Q}{D^3})^n + \tau_0)}{\rho Q^3}}_{\text{LHS}} = \underbrace{a\Big(\frac{\Delta P L^3}{T}\Big)^4 + b\Big(\frac{\Delta P L^3}{T}\Big)^2}_{\text{RHS}} \tag{14}$$

The given generalized equation is nonlinear and solving for the flow rate, Q, requires the use of numerical methods due to its implicit nature. In this study, an iterative numerical method was employed to solve the equation and determine the value of Q.

In order to adjust the motor speed, the difference between the calculated left-hand side (LHS) and right-hand side (RHS) of Equation (14) is utilized. When the LHS and RHS are equal, in other words have zero difference, that means that the system reached to a state that lies on the correlation curve.

Figure 13 illustrates the method for iteratively solving Equation (14). The controller adjusts the angular velocity of the screw motor (ω) as it influences the dynamics of other parameters within the system, which include pressure (ΔP), motor torque

(T), and flow rate (Q). The controller adjusts the motor speed until LHS equals RHS. If there are changes in pressure or torque (RHS), the system can adapt by changing the rotation speed (ω). The closed-loop ensures that the flow rate remains within the desired range throughout the extrusion process.

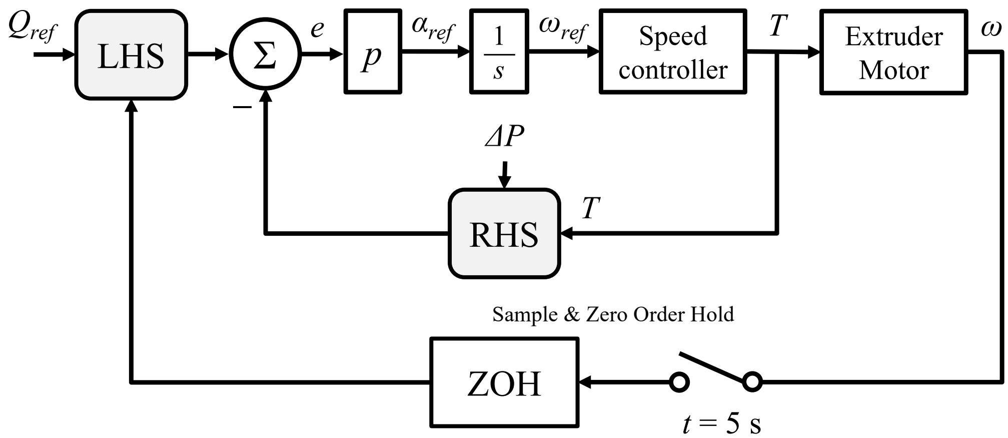

Figure 13: The controller block diagram to regulate the angular velocity, ω, of the screw motor. ω_{ref} is the reference angular velocity provided to the internal speed controller of the motor driver. α_{ref} is the reference angular acceleration. p is the proportional gain of the controller.

2.8 Controller Implementation

To regulate the extrusion flow rate, the controller was implemented in MATLAB Simulink. The controller aims to equalize the RHS and LHS of Equation (14) by adjusting the speed of the screw motor based on pressure sensor (ΔP) and torque (T) measurements.

The system is initialized with an arbitrary motor speed (ω_0) and filled with the specified cement batch. The Herschel-Bulkley parameters (τ, k, n) of the cement batch and the desired flow rate value, Q_{ref} were provided as constants.

Considering the variations in the extrusion process speed, the pressure and torque measurements also exhibit changes that reflect the corresponding effects on the cement. These changes occur over time, and the dynamics of the system include a transport delay. To address this delay, a sampled-data proportional control strategy is incorporated alongside the iterative solution. This control strategy samples the input signal at discrete time intervals and calculates the control input using a proportional gain, p. With proper gain and sampling period selection the controller can achieve zero steady-state error [76].

In systems with slow dynamics like this one, rapid changes in the control input can lead to output saturation and instability. To mitigate this issue, a sample and zero-order hold (ZOH) technique was employed. The ZOH holds the motor speed (ω) constant for a fixed time interval between samples, allowing the control response to stabilize before the next sample is taken. This improves overall stability and performance of the control system.

A thorough set of tests were carried out utilizing holding times ranging from 0.5 seconds to 10 seconds in order to establish the ideal holding time for the Zero-Order Hold (ZOH) approach. A sensitive trade-off between convergence time and stability affects how the system behaves. On the one hand, shorter holding times speed up convergence but impair stability, which could result in a failed convergence. Higher holding times, on the other hand, improve system stability while also delaying convergence, which makes them less useful for real-time control. This study set out to determine the best holding period, one that increases stability while reducing convergence time.

The system was first put to the test using a 0.5 second holding period. The motor speed was constant for 0.5 seconds during each iteration. But it soon became clear that the dynamics of this system required more time than this to reach steady—state. The pressure sensors, which are intended to track changes in motor speed, were unable to reliably record these differences within such a short time frame. As a result, the system showed instability, and convergence occasionally failed to occur. This discovery demonstrated the requirement for a longer holding period.

Subsequently, the system was tested with a significantly longer holding time of 10 seconds. This extended duration allowed the system to stabilize more effectively, resulting in improved convergence rates. However, the trade-off became apparent as the convergence time increased substantially, reaching up to 5 minutes in certain cases. Such extended convergence times rendered the control system impractical for real-time applications, prompting further investigation into finding the optimal balance.

To explore a range of options, various holding times between 0.5 seconds and 10 seconds were examined. Each test was carefully analyzed, considering both convergence time and stability. After meticulous evaluation, a holding time of 5 seconds emerged as the best compromise. This duration struck a balance, providing an average convergence time of 2 minutes with a remarkable 100% convergence efficiency. This result indicated that the system achieved stable and reliable convergence within a reasonable timeframe, making the 5-second holding time the optimal choice for the ZOH method in this particular application.

CHAPTER III

EXPERIMENTAL VERIFICATION AND DISCUSSION

The experimental procedure to verify the method involves comparison of two measures: the actual flow rate measured by the gravimetric method and the estimated flow rate derived from the established equation (14). To simplify the terminology, the gravimetric flow rate will be referred to as the *measured flow rate*, Q_{meas}, and the flow rate calculated using the established equation will be refereed as the *derived flow rate*, $Q_{derived}$.

3.1 Performance Evaluation of Derived Flow Rate

In this study, an experimental setup was designed to evaluate the effectiveness and performance of a proposed flow rate control strategy using various cement-based mixtures with different rheological parameters.The setup was utilized to conduct printing tests under different flow rates ranging from 15 to 30 g/s. During these test trials, the rotational speed of the screw, motor current, and pressure values were continuously recorded. The system's convergence was monitored, and once a steady state was achieved, the flow rate was measured before resetting the system. This iterative process was repeated until a significant amount of data was collected to enable conclusions regarding the system's performance.

The recorded data from one of these tests is presented in Figure 14. Figure 14-a shows the convergence status of the controller by comparing the RHS and LHS of the correlation equation. The rotational speed of the motor, shown in Figure 14-c, was adjusted by the controller to minimize the error between RHS and LHS, as depicted in Figure 14-b. The motor velocity is initially set to $w_0 = 2$ rpm, and reached a steady state around 3 rpm with a standard deviation of 0.137 rpm. Figure 14-d displays the derived flow rate values observed during the test trial. The dashed horizontal line represents the reference flow rate value set at $\dot{m}_{ref} = 20$ g/s. The x-axis represents the time from 0 to 200 seconds, while the y-axis represents the derived flow rate, Q. Examining the plot, it is evident that initially, the derived flow rate deviates from the target flow rate, indicating an insufficient rotation rate. However, as time progresses and the screw rotation rate is adjusted, the derived value gradually changes and eventually fluctuates around the target value. Due to system dynamics, the flow rate tracking error monotonically decays to zero, while the convergence exhibits oscillatory behavior.

In figure 15 the collected derived flow rate data is visualized via histogram plot. Here x-axis shows the collected estimation data while the y-axis shows the element count. Furthermore, each plot was fitted with a histogram line to visualize the underlying distribution. The normality of these distributions was assessed through a chi-square fit goodness test, with a 5% significance level. A chi-square test of normality showed that the data associated with the 15 g/s test is consistent with a normal distribution, χ^2 (5, N = 577) = 3.4557, p = .63 . Similarly, the same test is applied to the other test condition data and the same outcome is observed with the results χ^2 (6, N = 772) = 2.67, p = .85 and χ^2 (7, N = 361) = 5.81, p = .56, χ^2 (8, N = 534) = 15.26, p = .0543 for test conditions 20, 25 and 30 g/s respectively.

Figure 16 presents the box plots illustrating the derived flow rate data collected throughout the experiments. The abscissa represents the target flow rates applied during the experiments, while the ordinate denotes the corresponding derived flow rate values. A dashed black line, with a slope of 1, serves as the reference line. Examining the box plots, several key observations can be made. The median values of the derived flow rate groups are calculated as 14.96, 19.10, 24.60, and 29.41 g/s for the target flow rates of 15, 20, 25, and 30, respectively. Notably, the medians closely align with the reference line, indicating a minimal deviation. Additionally,

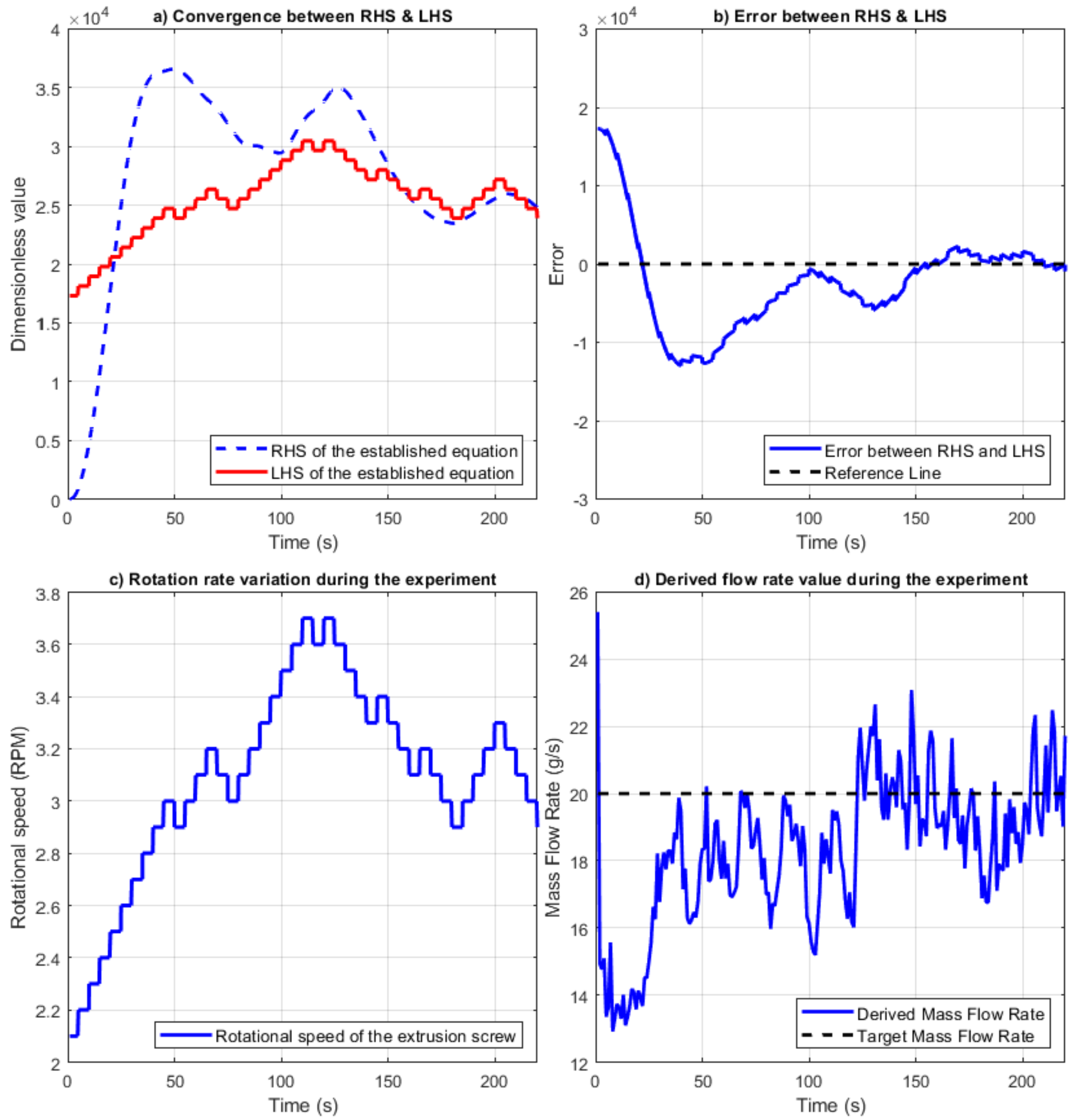

Figure 14: Recorded data of a flow rate control system test trial. a) The convergence status of the control system, the blue line depicts RHS, red line depicts LHS of the equality (13). b) The error progression between RHS and LHS of the equality during the experiment, the blue line represents the error value, and the black dashed line displays the reference error value as 0. c) The change in screw rotation speed during the experiment. d) The derived flow rate value during the experiment using equation (13), the blue line represents the derived flow rate value over time, the black dashed line represents the reference flow rate value of the experiment $Q_{ref} = 20$.

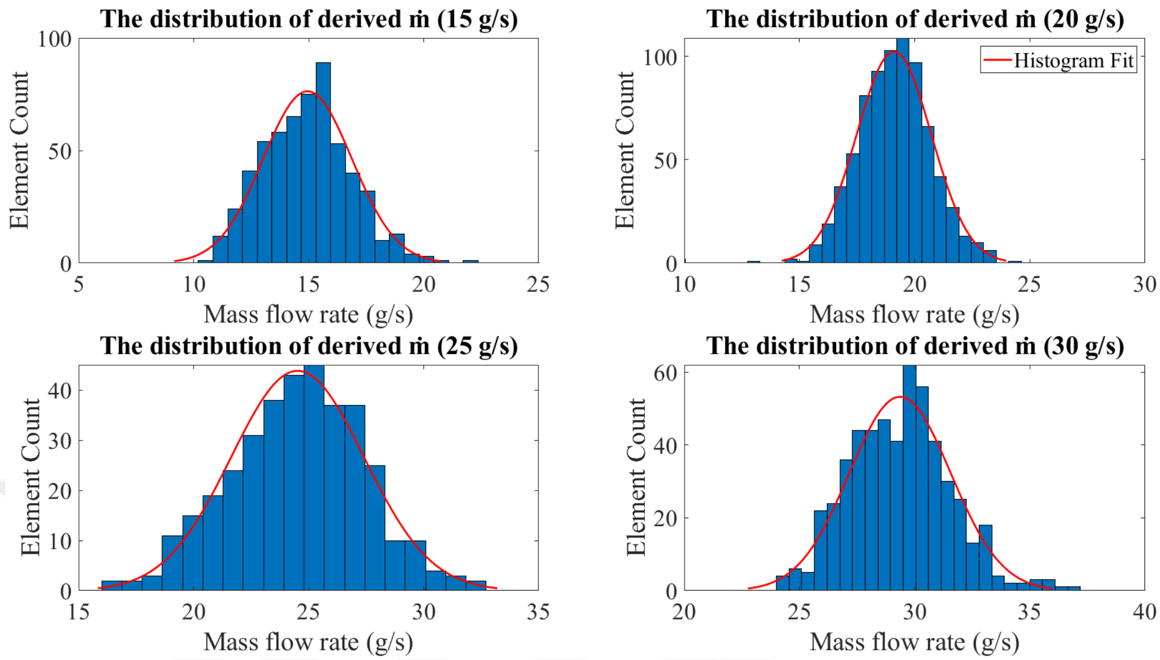

Figure 15: The histogram plots of collected signal data. Each plot shows a different group of data with a target flow rate value given in the title of the plot. The x-axis shows the flow rate data calculated from signal data. Y-axis shows the element count. The red line is the fitted histogram curve.

the quartile values for each estimation group are tightly clustered together, suggesting consistent distribution of the estimated data around the median value. Based on these findings, it can be concluded that the established control system effectively operates and successfully achieves the target flow rate value.

Figure 17 illustrates a collection of data sets presented as four subplots, each sharing the same color scheme. The different colors represent distinct experimental runs. Each subplot displays the derived mass flow value corresponding to the target flow rate indicated in its title. During the tests, all parameters, except the flow rate, are either known as geometric parameters or measured using related sensors or machines. By supplying all the parameters into the correlation equation, the flow rate value can be calculated for each time step, referred to as the "derived mass flow rate." These calculated values are then plotted on the same graph to observe the convergence behavior of the system under various conditions. The x-axis represents

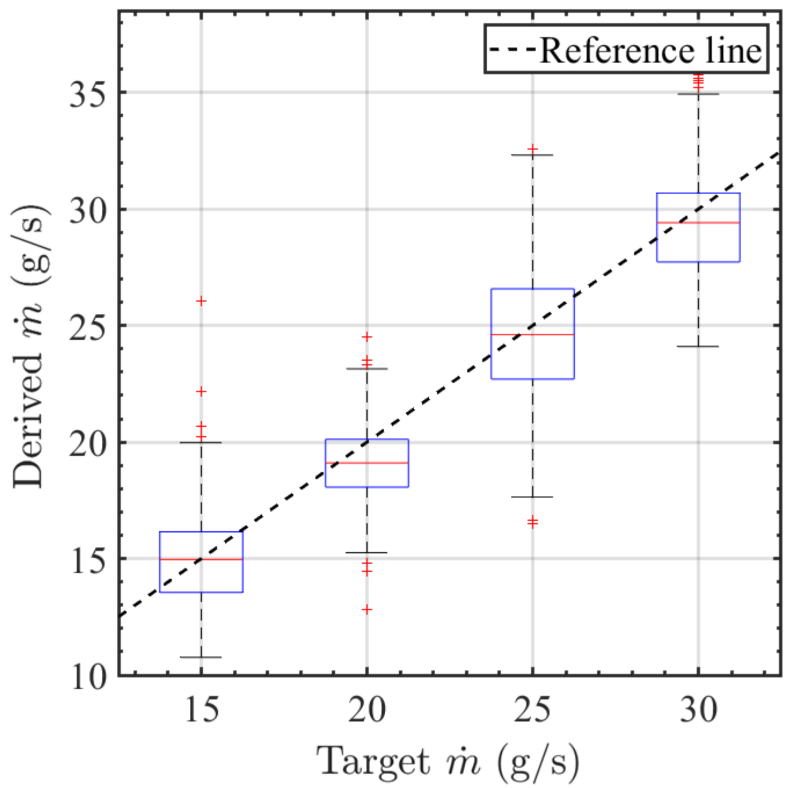

Figure 16: Box plot of derived flow rate values using the control system with respect to the target flow rates. The dashed line shows the reference line with the slope of 1. Derived flow rate : Flow rate calculated using the established equation (14), Target flow rate : The targeted flow rate of the respective group. For each box group; the red line shows the median value, the upper blue line shows the third quantile and the lower one shows the first quantile. The upper horizontal line shows the upper adjacent value while the lower one shows the lower adjacent. The red plus signs indicate the outliers.

the time during the experiment, ranging from 0 to 200 seconds, while the y-axis represents the derived mass flow rate values obtained from the correlation equation. Additionally, each plot includes a dashed reference line indicating the target flow rate value for each group.

Looking at these plots it can be observed that at the beginning of the experiments, the instantaneous flow rate is not equal to the target flow rate. However, as time progresses, the calculated flow rate from the signal changes due to the iterative procedure of the control system. Eventually, the signal data starts to fluctuate around the target flow rate value. This shows that the signal data coming from the control algorithm can successfully converge.

Another important aspect of this plot is the significance of the initial guess. In the tests conducted at a flow rate of 25 g/s, the initial guess was set at 2 rpm. However, based on those tests, it was found that the system actually required approximately 4 rpm to reach the target flow rate on the day of the experiment. This indicates that the initial guess for the rotation was significantly far from the converged value. As a result, the system took a long time to converge. The implication of this observation is that with a more accurate initial guess, the system has the potential to converge in a shorter duration. Alternatively, the system can be enhanced by employing higher precision sensors and reducing the 5-second delay, which would help improve this issue.

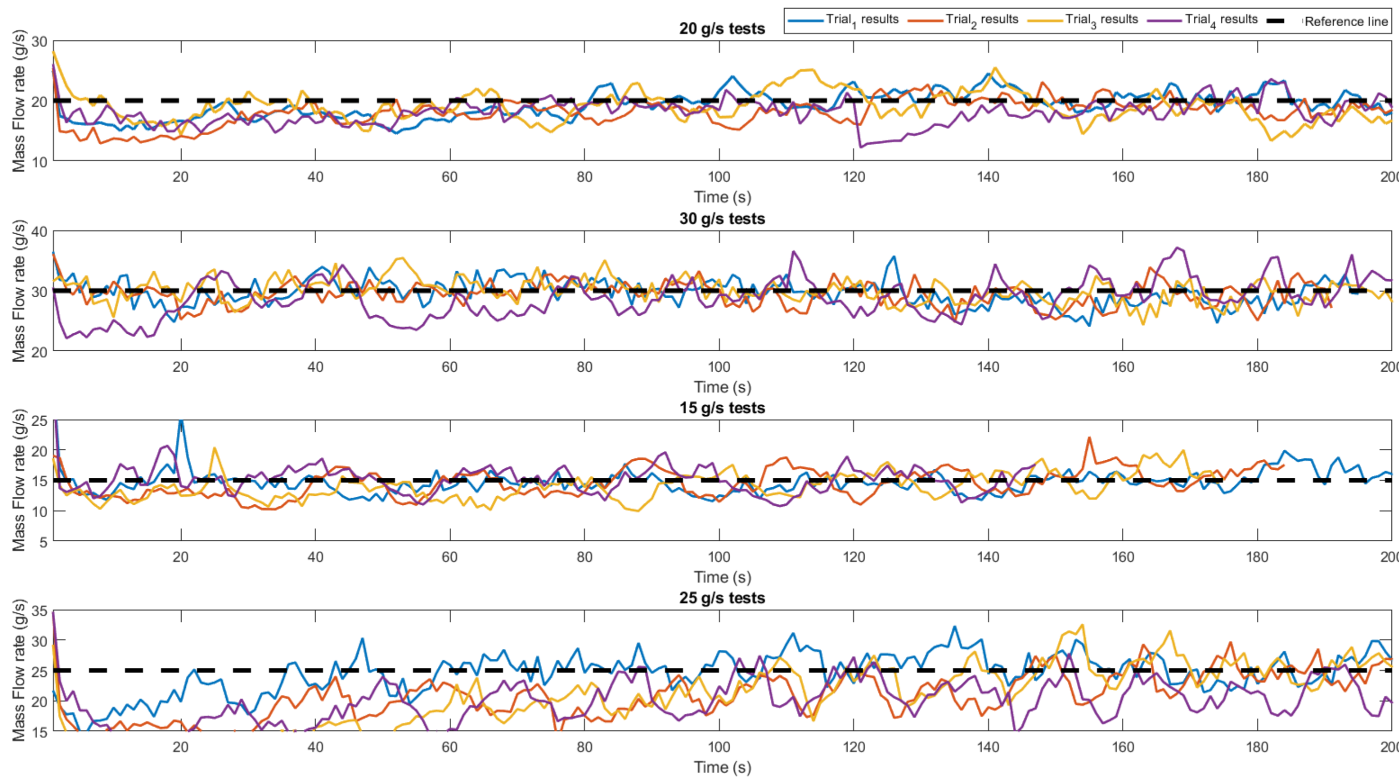

Figure 17: The subplots of collected signal data during experimental runs. Each subplot shows a collection of data for different target flow rates. Each trial is denoted with different colors. The x-axis shows the time. the y-axis shows the calculated flow rate from signal data.

3.2 Comparison of Measured and Derived Flow Rates

Table 4 presents a comprehensive summary of the results obtained from 17 experimental tests.The table showcases the measured and derived flow rates corresponding to a target flow rate, accompanied by their respective percent errors.

Each experiment reached a steady state, and material was extruded and collected for a duration of 30 seconds. The measured flow rate was calculated based on the collected material, while the derived flow rate was determined using the control method. The average error for the measured flow rate results was 6.7%, while it was 2.8% for the derived flow rate data.

The observed variations in the errors can be attributed to experimental uncertainties rather than factors related to the experimental conditions. These results demonstrate that the control system operates successfully, effectively maintaining the flow rate at the desired value with an acceptable level of error (i.e., below 10%) in both the derived and measured cases.

Figure 18 exhibits a comparison between the measured and derived flow rates through error bar plots. The error bars are generated using t-distribution rules for small sample sizes (n=4) with a confidence interval of 95%. On the graph, the x-axis represents the data obtained from the measurement method, while the y-axis represents the corresponding derived data. In each experiment, both the "measured" and "derived" flow rates are recorded. It is desirable for these two values to be as close as possible to ensure the proper functioning of the system. To assess the proximity of these values, a box plot is created. This box plot provides information about the closeness of the measured and derived flow rates. Additionally, the box plot can be used to evaluate the repeatability of the system, as it indicates the confidence range of the measurements.

The figure shows that the points where the measured and derived data intersect align closely with the reference line. This observation indicates that both the derived and measured solutions closely resemble the target value, demonstrating their excellent performance and near-identical behavior.

Table 4: Flow rate control model test results under different test conditions with gravimetric measurement of 30s sample time

Target Flow Rate (g/s)	Measured Sample Weight (g)	Measured Flow Rate (g/s)	Error of Measured Flow Rate (%)	Drived Flow Rate (g/s)	Error of Drived Flow Rate (%)
20	689.0	23.0	15.0	19.5	2.5
20	556.0	18.6	7.5	18.9	5.5
20	613.0	20.4	2.0	18.8	6.0
20	550.0	18.4	8.7	19.3	3.5
30	964.0	32.1	7.0	28.7	4.3
30	971.0	32.3	7.6	29.3	2.3
30	843.0	28.1	6.3	29.4	2.0
30	952.0	31.7	5.7	29.8	0.7
15	475.4	15.8	5.0	14.7	2.0
15	452.7	15.1	0.6	15.00	0.0
15	460.4	15.4	2.6	15.3	2.0
15	413.4	13.8	8.7	15.1	0.7
15	401.0	13.4	12.0	15.2	1.3
25	799.6	26.6	6.0	25.2	0.8
25	780.0	26.0	3.8	24.4	2.4
25	689.4	23.0	8.7	24.3	2.8
25	701.4	23.6	6.0	22.6	9.6
Average %Error	-	-	6.7	-	2.8

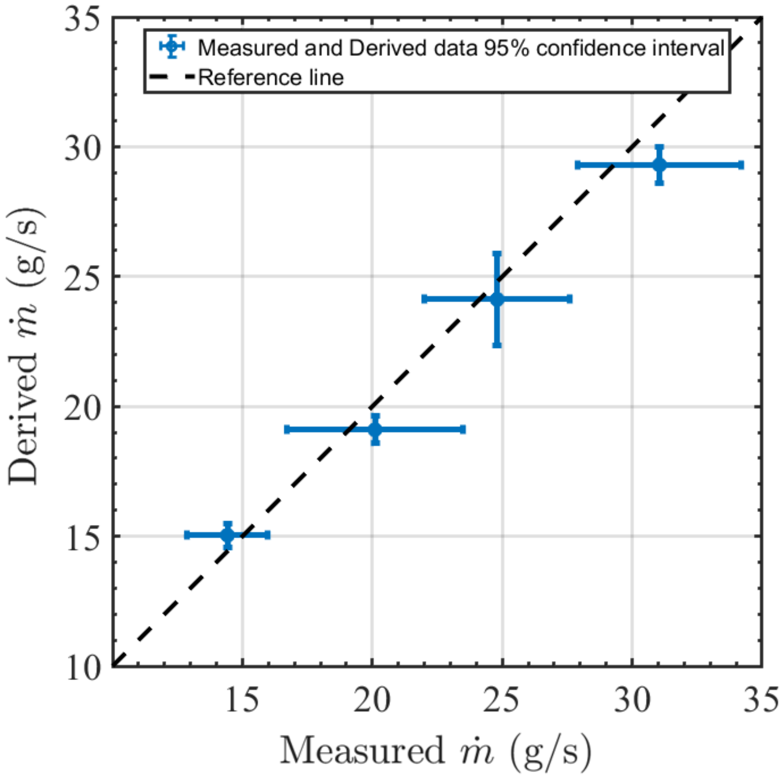

Figure 18: The error bar plot according to T-distribution. The x-axis shows the flow rate values obtained from measured data. The y-axis shows the flow rate values obtained from derived data. Measured flow rate: The flow rate values measured with the gravimetric measurement method, Derived flow rate: The flow rate values calculated using the established equation (14). The T-distribution with n=4 and 95% confidence interval is used. The dashed line is the reference line with the slope of 1

CHAPTER IV

CONCLUSIONS

3DCP is an advanced construction technology that is gaining increasing popularity as it offers numerous benefits. This new construction method has been proven to be more efficient, reliable, fast, and safe by several studies. However, the current application of the process lacks quality assessment technology which is reported to be one of the main reasons for application errors.

This thesis provides a brief introduction, highlighting the increasing popularity of automation in construction. One of the most popular topics in construction automation is 3D Concrete Printing (3DCP). The development steps of 3DCP, including Contour Crafting, D-Shape, and cement extrusion technologies, are briefly described with general information. Additionally, the current challenges in 3DCP applications, such as under filling and cold joint formation, are addressed, and possible reasons for these issues are discussed. It is concluded that the main reason for such problems is the lack of process quality control during operations, and the introduction of a control method can potentially resolve these issues.

Based on this outcome, previous studies on extrusion control systems are examined. Various control techniques are identified, including vibration-based methods to enhance product quality, toolpath control systems, height sensors for nozzle control, torque-based feedback control, and temperature-based control to account for system dynamics. However, it is determined that none of these studies fully address the rheological variances of the system, and there is still a need for an inline quality assessment technique that can account for rheological variations.

In light of this, the thesis takes a different approach by conducting non-dimensional analysis on the 3DCP process. The closely related and important parameters in the system are listed, and a total of 12 dimensionless numbers are formulated. This investigation aims to gain a better understanding of the system dynamics and introduce a universal analysis by removing the dimensional aspects.

A series of simulations is subsequently conducted to identify the most important parameters that exhibit significant differences when introducing cement with varying rheological behavior. To facilitate this analysis, a simple pump-screw type extrusion system is designed. The investigation also involves exploring suitable physical models to accurately simulate cement behavior. Following an evaluation of two different studies, the "Generalized power law" model is selected due to its widespread usage and ability to provide fast and reliable results. The chosen model is then validated through a series of test sequences. These sequences involve assessing the rheological behavior of cement samples using both simulation and a rheology machine. The results from the simulation and rheology machine are compared, revealing highly similar solutions and confirming the effectiveness of the selected physical model.

Further simulations are conducted at different rotation rates, using cement samples with distinct rheological behaviors. During these tests, various parameters such as torque, flow rate, shear rate, shear stress, and pressure are recorded. An investigation is conducted on the collected data to identify the important parameters. It is determined that the pressure drop, flow rate value, torque value, yield stress of the cement samples, and the dynamic viscosity of the cement samples are crucial parameters. These parameters have the potential to be utilized as a feedback system to create control mechanisms capable of distinguishing rheological variances.

Based on these outcomes, an experimental setup is designed to measure pressure, torque, and flow rate values during different experiments. The system is designed to mimic the simulation by employing a screw-pump extrusion method. The setup includes two pressure sensors to measure pressure drop, the torque value is derived from the current demanded by the motor driver, and the flow rate is measured using a gravimetric measurement method. The materials chosen for this setup are carefully designed to have a long setting time and minimal changes in rheological parameters over time. These materials undergo testing in 1-hour trial runs to confirm that their rheological parameters can be assumed constant during the trials.

Subsequently, the collected data is used to calculate the derived dimensionless numbers. The correlation between these dimensionless numbers is investigated until a promising relationship between two of them is discovered. Eventually, a correlation with a goodness of fit score of .96 is identified between two dimensionless numbers. This correlation is then utilized to develop a control system based on the correlation equation. After thorough exploration, it is determined that controlling the flow rate is the most practical and convenient option derived from the equation.

To regulate the flow rate, it is recognized that the equation needs to be solved explicitly. However, it is discovered that solving the equation for the flow rate results in an implicit equation. Therefore, an iterative numerical method is employed to solve the equation. Once the equation is solved using this iterative method, a control system utilizing the zero-order hold method is designed. Different holding periods ranging from 0.5 to 10 seconds are tested, and it is concluded that a 5-second hold time provides the most suitable system dynamics.

Subsequently, the established control technique is evaluated using the designated testing setup. For each test, a cement sample is introduced into the system. The system is initialized with a rotation rate value, and the rotation rate is adjusted to reach the desired flow rate. During the tests, pressure, torque, and other relevant parameters are recorded under the same test conditions. After some fluctuations, convergence is achieved in all test trials. Once convergence is attained, the flow rate is measured using the gravimetric method and recorded. These tests are repeated with different cement samples to assess the system's ability to successfully handle varying rheological behaviors.

The collected data is thoroughly investigated, focusing on the convergence behavior of the system through the use of plot representations. To facilitate clear terminology, the flow rate derived from the correlation equation is referred to as the "derived flow rate," while the flow rate measured using the gravimetric method is called the "measured flow rate." The distribution of the derived flow rate is analyzed using histogram plots. Furthermore, the closeness between the derived flow rate and the targeted flow rate is examined through box plots to gain insights into the data distribution.

Finally, a comparison is made between the measured and derived flow rates. The percent errors for each test trial are determined, and the average percent errors are calculated. An error bar plot, utilizing the T-distribution with n=4 and a 95% confidence interval, is utilized to assess the repeatability of the system.

Based on the collected data and the generated plots, a discussion is presented on the overall performance of the system and the applicability of the control solution.

In summary, this thesis proposes a novel method for controlling the flow rate in 3D Concrete Printing (3DCP), which utilizes a unique relationship between printing and rheological parameters. The control method involves a flow rate control algorithm that estimates the system's flow rate using pressure drop, demanded torque, and Herschel-Bulkley model parameters of the material. The test results validate that the system can maintain the flow rate at the desired value for various types of cement-based mixtures within an acceptable error range by adjusting the extrusion screw speed.

The major findings of this thesis are given below:

- A specially designed device has been developed for investigating the extrusion process for cement-based mixtures. The system allows for real-time sensor data collection and precise adjustment of the pumping speed.

- A unique relation between printing parameters and the rheological properties of the material is established with high correlation. By formulating an inclusive model that takes into account both the rheological parameters and the printing parameters, an equality describing the dynamics of the extrusion process was derived.

- The proposed control strategy was validated through experiments, and it was found that the control system effectively maintained the flow rate, with an average error of 6.7 percent.

In this study, the effectiveness of the proposed flow rate control strategy in 3DCP applications has been demonstrated. The validation of the performance of the system is held in both computational and experimental environments and the corresponding results are given in the aforementioned sections. It should be noted that the proposed flow rate control strategy represents just one application of the derived relationship. Further exploration of this relationship may uncover additional valuable applications.

For instance, the proposed control method, based on dimensionless analysis, has the potential to work with non-Newtonian fluids such as polymers. While this thesis primarily focuses on its application in 3DCP, the dimensionless nature of the derived equation allows for its utilization in controlling flow rates in polymer extrusion systems as well.

Additionally, the system can serve as a rheology machine. In this proposed system, the rheological parameters are provided as inputs. This enables the derivation of the instantaneous flow rate of the system, as it is the only unknown in the equation. Conversely, the equation can also be solved in reverse. The equation encompasses three rheological unknown parameters: the Herschel-Bulkley model parameters (yield stress τ, viscosity index k, and flow index n). To determine these three unknowns, the system can be extruded three times, and the flow rate can be measured. This measurement can be achieved using gravimetric methods, where the extrudate is collected in a container over a duration of time, and the mass flow rate is calculated by dividing the weight of the collected fluid by the elapsed time. Alternatively, an additional measurement device incorporating force sensors can be added to the system to continuously measure the flow rate. By employing the three flow rate measurements along with other measured quantities such as pressure and torque, the rheological parameters of the fluid being used can be determined. This feature allows the system to be utilized as an alternative rheology machine.

These represent two distinct usage ideas for this system. Further investigation in this field can unveil additional potential areas of application.

REFERENCES

[1] G. H. Ahmed, "A review of "3d concrete printing": Materials and process characterization, economic considerations and environmental sustainability," *Journal of Building Engineering*, vol. 66, p. 105863, 2023.

[2] V. J and P. Singh, "Chapter 9 - comparative analysis of concrete 3d printing and conventional construction technique for housing," *Woodhead Publishing*, pp. 177–190, 2023.

[3] M. Zhang, R. Xu, H. Wu, J. Pan, and X. Luo, "Human–robot collaboration for on-site construction," *Automation in Construction*, vol. 150, p. 104812, 2023.

[4] J. J. Magoua, F. Wang, N. Li, and D. Fang, "Incorporating the human factor in modeling the operational resilience of interdependent infrastructure systems," *Automation in Construction*, vol. 149, p. 104789, May 2023.

[5] R. Driessel and L. Moench, "An integrated scheduling and automated material handling approach for complex manufacturing systems," *International Conference on Industrial Engineering and Engineering Management, Singapore, Dec 08-11, 2008*, vol. 112, pp. 826–830, 2008.

[6] M. Spindler, T. Aicher, D. Schuetz, B. Vogel-Heuser, and W. A. Guenthner, "Modularized control algorithm for automated material handling systems," *19th IEEE International Conference on Intelligent Transportation Systems (ITSC), Rio de Janeiro, Brazil, Nov 01-04*, pp. 2644–2650, 2016.

[7] M. Taylor, S. Wamuziri, and I. Smith, "Automated construction in japan," *Proceedings of the institution of civil engineers-Civil engineering*, vol. 156, pp. 34–41, FEB 2003.

[8] W. Hu, J. Dong, and N. Xu, "Multi-period planning of integrated underground logistics system network for automated construction-demolition-municipal waste collection and parcel delivery: A case study," *Journal of cleaner production*, p. 129760, 2022.

[9] Y. Gamil, J. Nilimaa, T. Najeh, and A. Cwirzen, "Formwork pressure prediction in cast-in-place self-compacting concrete using deep learning," *Automation in Construction*, vol. 151, p. 104869, 2023.

[10] A. Mostafavi and Y.-J. Cha, "Deep learning-based active noise control on construction sites," *Automation in Construction*, vol. 151, p. 104885, 2023.

[11] Z. Ma, Y. Liu, and J. Li, "Review on automated quality inspection of precast concrete components," *Automation in Construction*, vol. 150, p. 104828, 2023.

[12] Y. Liu and Y. Bao, "Real-time remote measurement of distance using ultra-wideband (uwb) sensors," *Automation in Construction*, vol. 150, p. 104849, 2023.

[13] R. A. Buswell, W. L. De Silva, S. Z. Jones, and J. Dirrenberger, "3d printing using concrete extrusion: A roadmap for research," *Cement and Concrete Research*, vol. 112, pp. 37–49, 2018.

[14] S. Nehme and A. Abeidi, "3d concrete printing: review," *Epitoanyag-Journal of silicate-based and composite materials*, vol. 74, no. 5, pp. 183–187, 2022.

[15] F. P. Bos, Z. Y. Ahmed, R. J. M. Wolfs, and T. A. M. Salet, "3d printing concrete with reinforcement," in *High Tech Concrete: Where Technology and Engineering Meet*, pp. 2484–2493, Springer International Publishing, Aug. 2017.

[16] C. Holt, L. Edwards, L. Keyte, F. Moghaddam, and B. Townsend, "Chapter 17 - Construction 3D Printing," *3D Concrete Printing Technology*, pp. 349–370, 2019.

[17] T. Salet and R. Wolfs, "Potentials and challenges in 3d concrete printing," pp. 8–13, Research Publishing, 2016.

[18] J. Pegna, "Exploratory investigation of solid freeform construction," *Automation in Construction*, vol. 5, pp. 427–437, 1997.

[19] B. Khoshnevis, A. Carlson, N. Leach, and M. Thangavelu, "Contour crafting simulation plan for lunar settlement infrastructure build-up," *Earth and Space*, pp. 1458–1467, 2012.

[20] Alchaar, "Evaluation of 3d concrete printing in the united arab emirates. master's thesis, american university of sharjah, united arab emirates," 2020.

[21] A. K. Al-Tamimi, H. H. Alqamish, A. Khaldoune, H. Alhaidary, and K. Shirvanimoghaddam, "Framework of 3d concrete printing potential and challenges," *Buildings*, vol. 13, p. 827, 2023.

[22] E. Dini, M. Chiarug, and R. Nannini, "Method and device for building automatically conglomerate structures. u.s. patent 20080148683," 2008.

[23] J. Xiao, S. Zou, Y. Yu, Y. Wang, T. Ding, Y. Zhu, J. Yu, S. Li, Z. Duan, Y. Wu, and L. Li, "3d recycled mortar printing: System development, process design, material properties and on-site printing," *JOURNAL OF BUILDING ENGINEERING*, vol. 32, p. 101779, NOV 2020.

[24] V. N. Nerella, M. Nather, A. Iqbal, M. Butler, and V. Mechtcherine, "Inline quantification of extrudability of cementitious materials for digital construction," *Cement & concrete composites*, vol. 95, pp. 260–270, JAN 2019.

[25] A. V. Rahul, M. Santhanam, H. Meena, and Z. Ghani, "3d printable concrete: Mixture design and test methods," *Cement & concrete composites*, vol. 97, pp. 13–23, MAR 2019.

[26] Y. Chen, S. He, Y. Gan, O. Çopuroğlu, F. Veer, and E. Schlangen, "A review of printing strategies, sustainable cementitious materials and characterization methods in the context of extrusion-based 3d concrete printing," *Journal of Building Engineering*, vol. 45, p. 103599, 2022.

[27] S. C. Paul, Y. W. D. Tay, B. Panda, and M. J. Tan, "Fresh and hardened properties of 3d printable cementitious materials for building and construction," *Archives of Civil and Mechanical Engineering*, vol. 18, pp. 311–319, Jan. 2018.

[28] T. S. Rushing, P. B. Stynoski, L. A. Barna, G. K. Al-Chaar, J. F. Burroughs, J. D. Shannon, M. A. Kreiger, and M. P. Case, "Chapter 7 - Investigation of Concrete Mixtures for Additive Construction," *3D Concrete Printing Technology*, pp. 137–160, 2019.

[29] R. Jayathilaka, P. Rajeev, and J. Sanjayan, "Rheometry for concrete 3d printing: A review and an experimental comparison," *Buildings*, vol. 12, p. 1190, 08 2022.

[30] R. Buswell, J. Xu, D. De Becker, J. Dobrzanski, J. Provis, J. T. Kolawole, and P. Kinnell, "Geometric quality assurance for 3d concrete printing and hybrid construction manufacturing using a standardised test part for benchmarking capability," *Cement and concrete*, vol. 156, p. 106773, JUN 2022.

[31] S. Ketel, G. Falzone, B. Wang, N. Washburn, and G. Sant, "A printability index for linking slurry rheology to the geometrical attributes of 3d-printed components," *Cement and Concrete Composites*, vol. 101, pp. 32–43, 2019. Grand Challenges in Construction Materials 2016.

[32] R. J. M. Wolfs, F. P. Bos, E. C. F. van Strien, and T. A. M. Salet, "A real-time height measurement and feedback system for 3d concrete printing," in *High Tech Concrete: Where Technology and Engineering Meet* (D. Hordijk and M. Luković, eds.), (Cham), pp. 2474–2483, Springer International Publishing, 2018.

[33] P. F. Yuan, Q. Zhan, H. Wu, H. S. Beh, and L. Zhang, "Real-time toolpath planning and extrusion control (rtpec) method for variable-width 3d concrete printing," *Journal of Building Engineering*, vol. 46, p. 103716, 2022.

[34] T. A. M. Salet, Z. Y. Ahmed, F. P. Bos, and H. L. M. Laagland, "Design of a 3d printed concrete bridge by testing," *Virtual and Physical Prototyping*, vol. 13, no. 3, pp. 222–236, 2018.

[35] N. Ducoulombier, P. Carneau, R. Mesnil, L. Demont, J.-F. Caron, and N. Roussel, ""the slug test": Inline assessment of yield stress for extrusion-based additive manufacturing," pp. 216–224, 2020.

[36] L. Reiter, T. Wangler, A. Anton, and R. J. Flatt, "Setting on demand for digital concrete – principles, measurements, chemistry, validation," *Cement and Concrete Research*, vol. 132, p. 106047, 2020.

[37] S. Paul, B. Panda, J. Lim, N. A. Noor Mohamed, M. Tan, and Y. W. D. Tay, "Automation of robotic concrete printing using feedback control system," in *2017 Proceedings of the 34rd ISARC, Taipei, Taiwan*, pp. 276–280, 06 2017.

[38] A. Kazemian and B. Khoshnevis, "Real-time extrusion quality monitoring techniques for construction 3d printing," *Construction and Building Materials*, vol. 303, p. 124520, 08 2021.

[39] K. Gowers and S. Millard, "Measurement of concrete resistivity for assessment of corrosion severity of steel using wenner technique," *ACI Materials Journal*, vol. 96, pp. 536–541, 1999.

[40] S. Feliu, C. Andrade, J. González, and C. Alonso, "A new method for in-situ measurement of electrical resistivity of reinforced concrete," *Materials and Structures*, vol. 29, no. 6, p. 362 – 365, 1996.

[41] A. Ramezanianpour, A. Kazemian, M. Moghaddam, F. Moodi, and A. Ramezanianpour, "Studying effects of low-reactivity ggbfs on chloride resistance of conventional and high strength concretes," *Materials and Structures*, vol. 49, 07 2015.

[42] J. G. Sanjayan, R. I. Jayathilakage, and P. T. Rajeev, "Vibration induced active rheology control for 3d concrete printing," *Cement and Concrete Research*, vol. 140, p. 106293, 2021.

[43] V. Mechtcherine, F. Bos, A. Perrot, W. L. da Silva, V. Nerella, S. Fataei, R. Wolfs, M. Sonebi, and N. Roussel, "Extrusion-based additive manufacturing with cement-based materials – production steps, processes, and their underlying physics: A review," *Cement and Concrete Research*, vol. 132, p. 106037, 2020.

[44] R. Jayathilakage, P. Rajeev, and J. Sanjayan, "Yield stress criteria to assess the buildability of 3d concrete printing," *Construction and Building Materials*, vol. 240, p. 117989, 2020.

[45] R. Wolfs, F. Bos, and T. Salet, "Early age mechanical behaviour of 3d printed concrete: Numerical modelling and experimental testing," *Cement and Concrete Research*, vol. 106, pp. 103–116, 2018.

[46] J. Kruger, S. Zeranka, and G. van Zijl, "3d concrete printing: A lower bound analytical model for buildability performance quantification," *Automation in Construction*, vol. 106, p. 102904, 2019.

[47] R. Buswell, R. Soar, A. Gibb, and A. Thorpe, "Freeform construction: Mega-scale rapid manufacturing for construction," *Automation in Construction*, vol. 16, no. 2, pp. 224–231, 2007.

[48] T. Marchment and J. Sanjayan, "Mesh reinforcing method for 3d concrete printing," *Automation in Construction*, vol. 109, p. 102992, 2020.

[49] T. Marchment, J. Sanjayan, and M. Xia, "Method of enhancing interlayer bond strength in construction scale 3d printing with mortar by effective bond area amplification," *Materials & Design*, vol. 169, p. 107684, 2019.

[50] V. Mechtcherine, V. N. Nerella, and K. Kasten, "Testing pumpability of concrete using sliding pipe rheometer," *Construction and Building Materials*, vol. 53, pp. 312–323, 2014.

[51] N. Roussel, "Rheological requirements for printable concretes," *Cement and Concrete Research*, vol. 112, pp. 76–85, 2018. SI : Digital concrete 2018.

[52] A. Wolfs, "Konstruktivistische sichtweisen in der logopädischen therapie - zielgerichtete patientenorientierung durch eine einheitliche begriffswelt," *Springer Fachmedien Wiesbaden*, pp. 1–4, 2019.

[53] R. Jayathilakage, P. Rajeev, and J. Sanjayan, "Predication of strength-based failure in extrusion-based 3d concrete printing," *RILEM*, vol. 23, pp. 391–399, 2019.

[54] A. Suiker, "Mechanical performance of wall structures in 3d printing processes: Theory, design tools and experiments," *International Journal of Mechanical Sciences*, vol. 137, pp. 145–170, 2018.

[55] A. Suiker, R. Wolfs, S. Lucas, and T. Salet, "Elastic buckling and plastic collapse during 3d concrete printing," *Cement and Concrete Research*, vol. 135, p. 106016, 2020.

[56] G. Grampeix, N. Roussel, and J. Dupoirier, "Internal vibration and viscous concrete: application and prediction of the radius of action," *Rheology and processing of construction materials, RILEM Proceedings PRO*, vol. 90, pp. 123–130, 2013.

[57] K. Lesage, "Interactions between cement and combined concrete admixtures: the influence of cement paste rheology," *Cement and Concrete Research*, vol. 29, pp. 1159–1165, 2014.

[58] H. Hedlund and P. Groth, "Air cooling of concrete by means of embedded cooling pipes-part i: Laboratory tests of heat transfer coefficients," *Materials and Structures*, vol. 31, pp. 329–334, 1998.

[59] J. J. Soto-Bernal, R. Gonzalez-Mota, I. Rosales-Candelas, and J. A. Ortiz-Lozano, "Effects of static magnetic fields on the physical, mechanical, and microstructural properties of cement pastes," *Advances in Materials Science and Engineering*, vol. 2015, pp. 1–9, 2015.

[60] S. D. Nair and R. D. Ferron, "Set-on-demand concrete," *Cement and Concrete Research*, vol. 57, pp. 13–27, 2014.

[61] S. Muthukrishnan, S. Ramakrishnan, and J. Sanjayan, "Buildability of geopolymer concrete for 3d printing with microwave heating," in *Second RILEM International Conference on Concrete and Digital Fabrication* (F. P. Bos, S. S. Lucas, R. J. Wolfs, and T. A. Salet, eds.), pp. 926–935, 2020.

[62] G. H. Tattersall and P. H. Baker, "The effect of vibration on the rheological properties of fresh concrete," *Magazine of Concrete Research*, vol. 40, no. 143, pp. 79–89, 1988.

[63] G. H. Tattersall and P. H. Baker, "An investigation on the effect of vibration on the workability of fresh concrete using a vertical pipe apparatus," *Magazine of Concrete Research*, vol. 41, no. 146, pp. 3–9, 1989.

[64] C. Hu and F. de Larrard, "The rheology of fresh high-performance concrete," *Cement and Concrete Research*, vol. 26, no. 2, pp. 283–294, 1996.

[65] R. Basterfield, C. Lawrence, and M. Adams, "On the interpretation of orifice extrusion data for viscoplastic materials," *Chemical Engineering Science*, vol. 60, no. 10, pp. 2599–2607, 2005.

[66] A. Clarke, B. Kha, and G. McNally, "Viscosity control for extrusion processes using recycled polymers," in *Proceedings of the Second International Conference on Advances in Mechanical and Automation Engineering - MAE 2015*, pp. 45–49, Institute of Research Engineers and Doctors, Apr. 2015.

[67] M. McAfee and G. McNally, "Real-time measurement of melt viscosity in single-screw extrusion," *Transactions of the Institute of Measurement and Control*, vol. 28, no. 5, pp. 481–497, 2006.

[68] V. Mechtcherine, F. Bos, A. Perrot, W. L. da Silva, V. Nerella, S. Fataei, R. Wolfs, M. Sonebi, and N. Roussel, "Extrusion-based additive manufacturing with cement-based materials – production steps, processes, and their underlying physics: A review," *Cement and Concrete Research*, vol. 132, p. 106037, 2020.

[69] N. Roussel, A. Gram, M. Cremonesi, L. Ferrara, K. Krenzer, V. Mechtcherine, S. Shyshko, J. Skocec, J. Spangenberg, O. Svec, L. N. Thrane, and K. Vasilic, "Numerical simulations of concrete flow: A benchmark comparison," *Cement and Concrete Research*, vol. 79, pp. 265–271, 2016.

[70] C. Karakurt, A. O. Çelik, C. Yılmazer, V. Kiriççi, and E. Özyaşar, "Cfd simulations of self-compacting concrete with discrete phase modeling," *Construction and Building Materials*, vol. 186, pp. 20–30, 2018.

[71] A. Perrot, D. Rangeard, V. N. Nerella, and V. Mechtcherine, "Extrusion of cement-based materials - an overview," *RILEM Technical Letters*, vol. 3, p. 91–97, Feb. 2019.

[72] H. Chen, D. Zhang, P. Chen, N. Li, and A. Perrot, "A review of the extruder system design for large-scale extrusion-based 3d concrete printing," *Materials*, vol. 16, no. 7, 2023.

[73] D. O. Kazmer, C. M. Grosskopf, D. Rondeau, and V. Venoor, "Design and evaluation of general purpose, barrier, and multichannel plasticating extrusion screws," *Polymer Engineering & Science*, vol. 60, no. 4, pp. 752–764.

[74] E. M. Aydin, B. Kara, Z. B. Bundur, N. Ozyurt, O. Bebek, and M. Ali Gulgun, "A comparative evaluation of sepiolite and nano-montmorillonite on the rheology of cementitious materials for 3d printing," *Construction and Building Materials*, vol. 350, p. 128935, 2022.

[75] M. Azima and Z. B. Bundur, "Influence of sporasarcina pasteurii cells on rheological properties of cement paste," *Construction and Building Materials*, vol. 225, pp. 1086–1097, 2019.

[76] S. Xu and C. Li, "Critical sampling period for sampled-data pi control systems," in *2022 41st Chinese Control Conference (CCC)*, pp. 827–832, 2022.

VITA

In his early years, Oğulcan had the privilege of attending elementary school at Private Sanko Schools, and he gratefully completed his high school education there in 2015. With deep appreciation, he enrolled at Özyeğin University, where he had the opportunity to pursue his passion for Mechanical Engineering, leading to the achievement of his Bachelor of Science degree in 2020. Continuing his academic journey, he was honored to earn a Master of Science degree in Mechanical Engineering from Özyeğin University in 2023.